Available online at www.sciencedirect.com

ScienceDirect

ELSEVIER

Journal of the European Ceramic Society 28 (2008) 505–529

ECERS

www.elsevier.com/locate/jeurceramsoc

Review

SnO_2, ZnO and related polycrystalline compound semiconductors: An overview and review on the voltage-dependent resistance (non-ohmic) feature

Paulo R. Bueno*, José A. Varela, Elson Longo

Instituto de Química, Universidade Estadual Paulista, P.O. Box 355, 14801-907 Araraquara, SP, Brazil

Received 2 November 2006; received in revised form 6 June 2007; accepted 15 June 2007
Available online 15 August 2007

Abstract

The present review describes mainly the history of SnO_2-based voltage-dependent resistors, discusses the main characteristics of these polycrystalline semiconductor systems and includes a direct comparison with traditional ZnO-based voltage-dependent resistor systems to establish the differences and similarities, giving details of the basic physical principles involved with the non-ohmic properties in both polycrystalline systems. As an overview, the text also undertakes the main difficulties involved in processing SnO_2- and ZnO-based non-ohmic systems, with an evaluation of the contribution of the dopants to the electronic properties and to the final microstructure and consequently to the system's non-ohmic behavior. However, since there are at least two review texts regarding ZnO-based systems [Levinson, L. M., and Philipp, H. R. *Ceramic Bulletin* 1985;**64**:639; Clarke, D. R. *Journal of American Ceramic Society* 1999;**82**:485], the main focus of the present text is dedicated to the SnO_2-based varistor systems, although the basic physical principles described in the text are universally useful in the context of dense polycrystalline devices. However, the readers must be careful of how the microstructure heterogeneity and grain-boundary chemistry are capable to interfere in the global electrical response for particular systems. New perspectives for applications, commercialization and degradation studies involving SnO_2-based polycrystalline non-ohmic systems are also outlined, including recent technological developments. Finally, at the end of this review a brief section is particularly dedicated to the presentation and discussions about others emerging non-ohmic polycrystalline ceramic devices (particularly based on perovskite ceramics) which must be deeply studied in the years to come, specially because some of these systems present combined high dielectric and non-ohmic properties. From both scientific and technological point of view these perovskite systems are quite interesting.
© 2007 Elsevier Ltd. All rights reserved.

Keywords: Varistors; SnO_2; ZnO

Contents

1. A brief history of non-ohmic devices 506
2. Basic concepts involving electric response of dense polycrystalline semiconductors 507
3. Grain-boundary capacitance in dense polycrystalline semiconductor devices 510
4. Microstructural comparisons between zinc oxide- and tin dioxide-based polycrystalline compound semiconductors 515
5. The effect of annealing at oxidizing and reducing atmospheres and microstructure heterogeneity 516
6. Tin dioxide- and titanium dioxide-based polycrystalline semiconductor 520
7. Similarities between metal oxide dense varistor and varistor-type sensor 521
8. Perovskite related polycrystalline non-ohmic devices 522
9. Future and prospects concerning technological application of tin dioxide-based varistors 524
10. Conclusions 527

Acknowledgments 527

References 527

* Corresponding author.
E-mail address: prbueno@iq.unesp.br (P.R. Bueno).

0955-2219/$ – see front matter © 2007 Elsevier Ltd. All rights reserved.
doi:10.1016/j.jeurceramsoc.2007.06.011

1. A brief history of non-ohmic devices

Non-ohmic devices are generally electronic ceramic materials whose electrical properties are greatly dominated by grain-boundary interface states. These non-ohmic ceramic devices are also known as “metal-oxide” varistors (variable resistors) whose applications are technologically important because of their electrical characteristics that enable them to be used as solid state switches with large-energy-handling capabilities. The varistors are also know as voltage-dependent resistors (VDR) because they show a highly nonlinear current–voltage (I– V) characteristic with a highly resistive state in the pre-breakdown region (also know as ohmic region) and large non-linearity coefficient $\alpha = \mathrm{d}\log I/\mathrm{d}\log V$ (see Fig. 1, in the breakdown region). Several materials with charged grain boundaries show to some extent such non-linearity phenomena.[3] Some examples are $SrTiO_3$,[4,5] TiO_2,[6,7,8,9,10] WO_3,[11,12] ZnO,[1,2] and SnO_2.[13,14,15] For $SrTiO_3$ and ZnO, the ‘varistor effect’ is optimized in commercial devices used for voltage surge protection and α values of the order of $\alpha \simeq 15$–35 or $\alpha \simeq 50$–200, respectively, have been observed. From a physical point of view, the nonlinearity in the I– V characteristic originates from the *bias* dependence of the interface charge, which control the barrier height and hence the current flow across the junction.

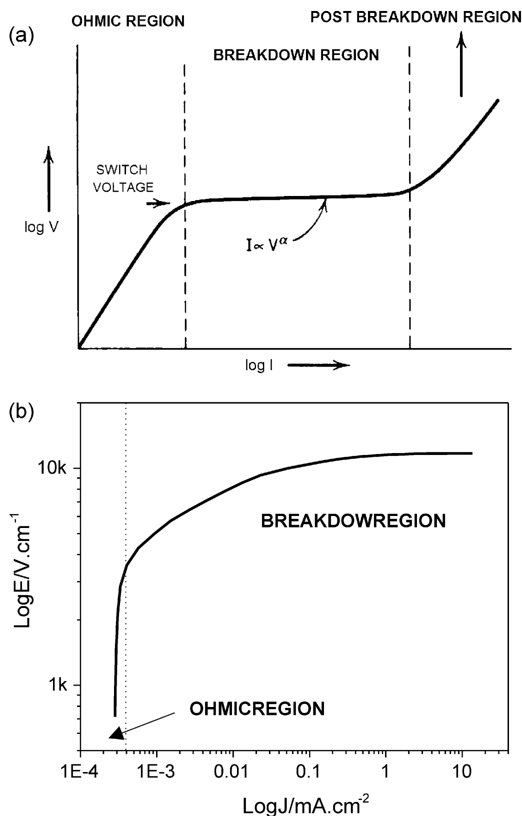

Fig. 1. (a) Schematic representation of a current–voltage features of a VDR (varistor) devices. When the applied voltage exceeds the nominal voltage (or breakdown voltage) the materials resistance strongly decreases, allowing the current to flow throughout of the polycrystalline material. A real current–voltage response of a VDR (SnO_2-based varistor) device is presented in part (b) of this figure. Note that just the ohmic and breakdown region is observed in (b).

The VDR’s I– V characteristics are similar to those of barrier-injection transit-time diodes but with much more current and handling capabilities.[16,17,18,19] Functionally, VDR are used in parallel with circuits to protect them from voltage surges. They are subject to a voltage below their switch voltage and pass only a leakage current. When the voltage of the circuit exceeds the switch voltage, for instance, during a voltage transient or surge, the VDR becomes highly conducting and draws the current through it. When the voltage return to normal, the VDR returns to its original highly resistive state. The use of such polycrystalline semiconductors to protect sensitive equipment from transient overvoltage is simple: the VDR component is directly connected across the power line in parallel with the load to be protected and the VDR component is chosen to have a switch voltage or breakdown voltage (this term is the most frequently used in the literature, although switch voltage is the most appropriate) slightly greater than the maximum design voltage applied to the system to be protected.

The first VDR polycrystalline ceramics were developed around early the 1930s by the Bell System and consisted of partially sintered compacts of SiC. A VDR system with very superior performance based on ZnO composition was announced in 1969 by Matsuoka,[20] although parallel developments were conducted in Russia in the early of 1950s.[21] In 1971 Matsuoka gave details of a ZnO-based polycrystalline VDR system describing many of the essential features of ZnO-based VDRs as known today.[17] After that, an extensive literature was created, establishing the scientific basis of VDRs as well as many of the key technological developments.[2,1,19,18,22,23,24,25] The VDR’s device behavior is not affected by the electrode configuration or electrode composition. Leads are generally attached by solder and the finished device may be encapsulated in a polymeric material. The schematic diagram of the device with its polycrystalline morphology and leads is depicted in Fig. 2.

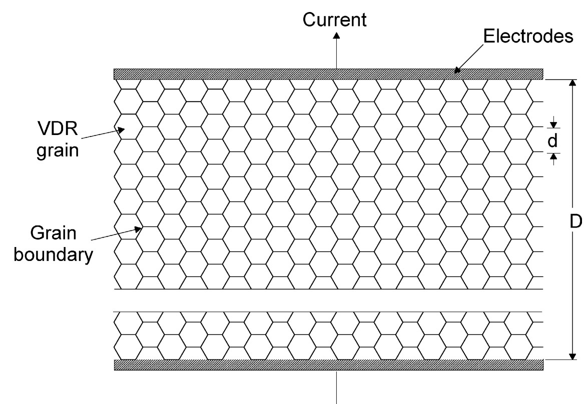

Fig. 2. Schematic representation of the microstructure of a ZnO or SnO_2 VDR devices. Grain of conduction ZnO or SnO_2, average $\bar{d}$, are generally completely surrounded by a segregation layer (few atomic layers thick) or precipitated phase (at least two order of magnitude higher than the segregated phase) according to the type of VDR or additive concentration used to fabrication. The electrodes are also represented and the current can flows as indicated. Note that real microstructure is not so regular, but both grain and grain-boundary region, as discussed herein, are intercalated in series along the length D.

The majority of the ZnO VDRs are based on bismuth-doped ZnO semiconductor, forming the ZnO bismuth-based varistor, which are the commonest varistor based composition and have been the subject of most of the research and development effort.[1,2] When CoO and Pr_6O_{11} is used in place of Bi_2O_3, very different microstructure and properties arise.[22,26] Nowadays, ZnO-based VDR systems are mass-produced in several countries, with applications ranging from power switching in electrical transmission systems to surge protection in automobile and semiconductor electronics. Non-ohmic conduction in ZnO varistors is explained by thermionic emission enhanced by barrier lowering at low fields with a combination of other mechanisms at high fields.[19]

Since the discovery of ZnO-based VDRs, there has been a steady search for alternative materials either to find VDRs with equivalent or superior properties and low-cost.[27,7,13] For systems based on polycrystalline semiconductors there are a variety of choices, however, at least two types of dopants are necessary: one that is soluble in the grain to affect the grain resistivity (to decrease it) and the other that is a larger or insoluble ion, that segregates at grain boundaries regions.

Pianaro et al.[28,13] were the first to use this concept to present, in 1995, a new VDR system based on SnO_2. Nowadays, SnO_2 is certainly one of the main polycrystalline ceramic candidates to compete with the traditional multicomponent ZnO-based VDRs, specially because of its more simple microstructure.[13] In the SnO_2-based VDR or varistor, introduced by Pianaro et al.,[28,13] CoO dopant is used to lead SnO_2 to a high degree of densification,[29,28] which makes it possible to define the varistors' behavior after the addition of Nb_2O_5 that acts as a donor in the bulk (decreasing the grain resistivity). It is important to emphasize that Co atoms also segregate at the grain boundary, which is also very important to define the non-ohmic behavior, as shall be discussed further herein.

A high non-linearity coefficient of ~ 41 was obtained in the $SnO_2\cdot$ CoO $\cdot Nb_2O_5$ (1.0 mol% of CoO and 0.05 mol% of Nb_2O_5) system when 0.05 mol% of Cr_2O_3 was added.[13] The major advantage of this system lies in its simple single-phase microstructure and its high electrical stability.[30,13] From a technological standpoint, these two characteristics are very important because they may increase the service life of the material and facilitate the control of its processing compared, for instance, with ZnO-based ceramics.[31] The disadvantage of SnO_2-based varistor is particularly involved with the needs of higher temperatures to prepare the blocks (at least 200° C higher).[33,29,32] This is expected since for SnO_2-based VDRs the sintering mechanism usually involves a solid-state sintering[29] and not the commonly liquid-phase sintering established for ZnO-based VDR compositions.[1,2]

Besides VDR systems, SnO_2 has been employed in a great number of technological applications, particularly in sensors, catalyzers, electro-optic equipment and photovoltaic cells,[34,35,36,37,38,39,40,41] most of which involve porous ceramics (sensors) and thin films.[42,43,44] The sensor properties of SnO_2 depend not only on such factors as the oxide's surface stoichiometry, the methodology used to prepare the powder, temperature and atmosphere of calcination but also, and mainly, on the high specific area deriving from the low densification of this oxide.[34,35,36,37,38,39,40,41]

It is generally assumed that low densification of pure SnO_2 is caused by the predominance of non-densifying mechanisms, such as evaporation-condensation.[34,39] These mechanisms, which are responsible only for the growth of grains and the formation of the necks between particles during sintering, do not promote densification. Hence, a variety of studies have been conducted with the purpose of obtaining SnO_2-based dense polycrystalline ceramics for a wide variety of applications. The densification obtained by Pianaro et al.[28,13] was in the order of 98.5% in relation to the theoretical density by adding 1.0 mol% of CoO to SnO_2. High density in polycrystalline ceramics is essential for high varistor properties, since the phenomena involved for good varistor properties occur in the region of the material's grain boundaries. Following the findings of Pianaro et al., several researchers began detailed studies of the densification of SnO_2 using dopants such as CoO, MnO_2,[29,32,45,47,46,50,104,48,52,49,33] TiO_2[53,54] and ZnO[27,55,56,57] while other authors dedicated themselves to study the electrical properties of this new polycrystalline system,[58,46,59,60,61,62] particularly those related to its non-ohmic characteristics. It is important to mention that a SnO_2 VDRs were concomitantly developed by Glot et al.,[63] however, the proposed composition was much less studied than that system presenting a simple composition introduced by Pianaro et al.,[13] probably because of the lower non-ohmic property achieved by the compositional system proposed by Glot et al.[63]

Fig. 3 illustrates the microstructural differences between high dense SnO_2 polycrystalline ceramics used in varistor applications (Fig. 3(b)), and the porous material used in gas sensor technology (Fig. 3(a)).

2. Basic concepts involving electric response of dense polycrystalline semiconductors

The *I versus V* (*I*– *V*) nonlinearity of non-ohmic ceramics is defined by the empirical equation:

$$I = KV^{\alpha}, \tag{1}$$

where I is the current, V the electrical potential, K a constant related to the material's microstructure, and α is the coefficient of nonlinearity. An example of varistor characteristics is given in Fig. 1. These polycrystalline ceramics are normally produced by solid-state reactions (generally by liquid phase in ZnO[2] or solid-state sintering in the majority of the situations for SnO_2-based systems[28,29,33]) after they have been conformed in a shape appropriate to their application. Eq. (1) is the so-called empirical varistor power law equation. If α is about the unity, the system will present an Ohmic response, i.e., the current is proportional to the applied voltage. As large the value of α more intense will be the non-ohmic response. The perfect VDR system is that in which the α value approach ∞, i.e., the current varies infinitely for small changes in the applied field.

The current–voltage characteristics of Eq. (1) are controlled by the existence of potential barrier at the grain boundaries.

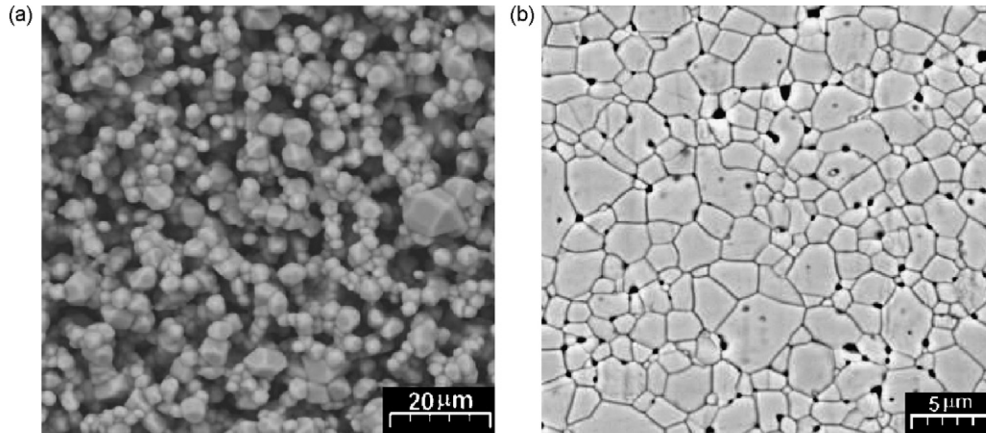

Fig. 3. (a) Typical microstructure of porous SnO_2-based polycrystalline ceramics. (b) Typical microstructure of highly dense SnO_2-based polycrystalline ceramics. Note that although the microstructure are very different, in both cases the junction contact plays a very important role in control the properties (more details are given in Section 7).

Some authors assume[2] that grain-boundary material in VDR systems consist of the same semiconducting material but contains defects in an increased concentration. Other authors assume that the grain-boundary material possess a different chemistry, i.e., it is formed by segregated dopants with "p-type nature" capable of enrich these region with oxygen species,[64,92,4] which is likely the main chemical specie responsible for the potential barrier formation.

In one or other case, the grain-boundary is treated as a junction in which the Fermi level of the bulk or grains are different from that of the layer between two grains, i.e., at grain-boundary region (see Fig. 4 (a), i.e., the illustration of a simple potential barrier with a thin layer between two grains). When the junction is formed and after the equilibrium to be reached, the Fermi level is the same along the junction so that the chemical (binding) energy gained by an electron occupying a trap state is equal to the electrostatic energy spent in moving an electron from the interior of the grains to the boundary. The result of this equilibrium is that the interface trapped electrons act as a sheet of negative charge at the boundary, leaving behind a layer of positively charged donor sites on either side of boundary, and create an electrostatic field with a barrier at the boundary. The chemistry that gives rise to this electrostatic potential barrier is discussed in Refs. 3,64,65 (for additional details see also Fig. 11 and related text on this review).

By solving the Poisson equation for the situation depicted in the last paragraph (i.e., ignoring deep bulk trap state or bulk energy levels) one may find

$$\phi_b = \frac{qN_{IS}^2}{2N_d k\epsilon_0}, \tag{2}$$

in which N_{IS} is the density of trapped charge in the interface (interfacial state density), k the relative permittivity (i.e., the permittivity of grains of the VDR system considered) and ϵ_0 is the permittivity of free space. Finally, q is the elementary charge.

The consideration of grain-boundary capacitance analysis, without bulk deep trap states contribution, can be done by taking into account the potential in the junctions as $\bar{V} = \bar{V}_f + \bar{V}_b$ (see Fig. 4). $\bar{V}_f$ is the forward band bending of the barrier (increasing

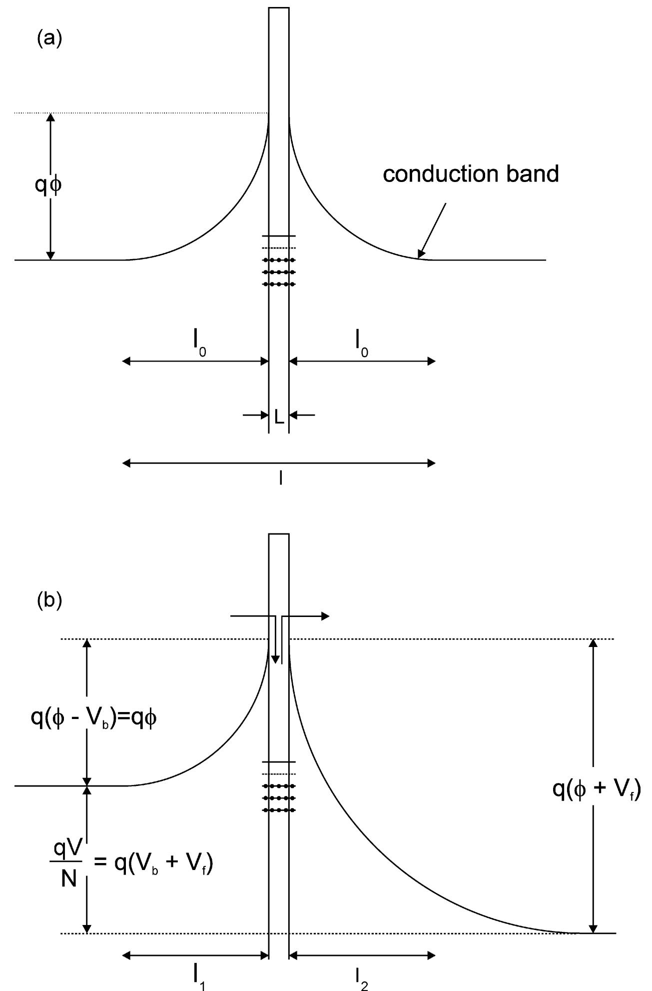

Fig. 4. Band structure of a single grain-boundary junction of a VDR device. (a) Scheme of the band structure without any bias potential applied (i.e., without a stationary V_{dc} potential or bias potential). (b) Schematic presentation with an potential bias applied (note the distortion of the potential barrier energy and of the break of energy levels symmetry caused by the applied V_{dc} potential). In this figure it is also important to note the representation of the thin layer generally observed in a simple junction. This thin layer is capable of trap electrons (the electronic density is higher compared to the bulk). The thickness of this layer is also a typical difference observed between ZnO- and SnO_2-based VDR systems.

of the barrier height at the negative side of the barrier polarization) meanwhile $\bar{V}_b$ is the backward band bending depletion (decreasing of the barrier height at the positive side of the barrier polarization). According to the scheme of band structure of the grain-boundary region described in Fig. 4, it is possible to consider the capacitance which depends on the length of the depletion layer, i.e., λ, as described by the following equation:

$$c_{gb} = \frac{k\epsilon_0 A_c}{(\lambda_f + \lambda_b)}, \tag{3}$$

in which A_c is the area of an individual junction, i.e., the area of the contact between two particles. This analysis is based in the so-called block model for VDR systems, which is a very useful approach to the understand of VDR behavior in a lot of metal oxide systems and sometimes provide resonable equivalent circuit representation of this polycrystalline devices. However, such model must be used carefully. Its limitation will be discussed further in this review.

Now, considering the band bending, each depression layer (of both side of the junctions) can be expressed as

$$\lambda_f = \left[\frac{2k\epsilon_0}{qN_d}\left(\phi_b + \bar{V}_f\right)\right]^{1/2}, \tag{4}$$

$$\lambda_b = \left[\frac{2k\epsilon_0}{qN_d}\left(\phi_b - \bar{V}_b\right)\right]^{1/2}. \tag{5}$$

If the donor concentration N_d is considered uniform, then the solution of the Poisson's equation for an individual junction capacitance or grain boundary, i.e., c^j_{gb}, leads to

$$\frac{1}{c^j_{gb}/A_c} = \left(\frac{2}{qk\epsilon_0 N_d}\right)^{1/2}\left[\left(\phi_b - \bar{V}_b\right)^{1/2} + \left(\phi_b + \bar{V}_f\right)^{1/2}\right]. \tag{6}$$

Note that Eq. (6) can be also derived from the combination of Eq. (3) with Eq. (4) and (5). Normally, it is possible to consider that $\bar{V}_f \gg \bar{V}_b$, implying that $\bar{V}_f = \bar{V}$ so that Eq. (6) turns into

$$\left(\frac{1}{c^j_{gb}} - \frac{1}{2c^j_{gb,0}}\right)^2 = \frac{2}{A_c^2 qk\epsilon_0 N_d}\left(\phi_b + \bar{V}_f\right), \tag{7}$$

in which $c^j_{gb,0}$ is the capacitance at zero bias voltage $\bar{V} = 0$.

From a plot of $(1/c^j_{gb} - 1/2c^j_{gb,0})^2$ versus $\bar{V}$ it is possible to calculate the N_d and potential barrier height, i.e., ϕ_b. When the macroscopic aspect is considered, i.e., the multi-junction aspect of the polycrystalline system is taken into account, the following relationship arises:

$$\frac{1}{C_{gb}} = \frac{p}{Ac^j_{gb}}, \tag{8}$$

in which A is the area of the electrode or of the cell. p is defined as the number of barrier per unit of length of the polycrystalline system considered, i.e., $p = \bar{d}/D$, being D the thickness of the device and $\bar{d}$ the average mean particle or grain size. Therefore, p is the number of barrier per unit of length of the polycrystalline device.

The p parameter is critical because it is capable of introducing serious and significant errors when the porosity is high in the polycrystalline system and the format of the grains is far from to be cubic. Another source of errors is related to the calculation of p, which in the majority of situations leads to the considerations of that all of grain–grain junctions form active potential barriers, i.e., the polycrystalline system is considered to be homogeneous (presenting homogeneous physical and chemistry characteristics of the junctions). Still it is important to observe, based on the discussion of the last paragraph, that the Eq. (8) is considered a mean value of the all active grain-boundary capacitance. Considering that $\bar{V} = p\bar{V}_f$ (according to the block model), the combination of Eq. (7) and (8) leads to a mean grain-boundary capacitance that can be rewritten as

$$\left(\frac{1}{C_{gb}} - \frac{1}{2C_{gb,0}}\right)^2 = \frac{2p^2\phi_b}{A^2 qk\epsilon_0 N_d} + \frac{2p\bar{V}}{A^2 qk\epsilon_0 N_d}, \tag{9}$$

$$\left(\frac{1}{C_{gb}} - \frac{1}{2C_{gb,0}}\right)^2 = \frac{2p^2}{A^2 qk\epsilon_0 N_d}\left(\phi_b + \frac{\bar{V}}{p}\right), \tag{10}$$

in which the $C_{gb,0}$ is the mean value of the grain boundary at a given zero bias dc potential.

The previous picture is totally in agreement with the Schottky diode picture of the potential barriers of VDR systems. Therefore, the current–voltage characteristic can be generally (i.e., phenomenologically) described by the following equation:

$$J = J_0\left(-\frac{q\phi_b}{k_B T}\right)\left[1 - \exp\left(-\frac{qV_f}{pk_B T}\right)\right], \tag{11}$$

in which J is the electronic flux due to electronic transport through the potential barrier and J_0 is a constant that can be a function of temperature and V_f is the potential of forward bias. To consider the macroscopic aspects, it is important to examine the potential dependence with the barrier. As the potential is given by $V = p(\bar{V}_b + \bar{V}_f)$ and p was already defined as the number of barrier per unit of length of the polycrystalline system, so that considering $\bar{V}_f \gg \bar{V}_b$, Eq. (11) turns into

$$J = J_0\left(-\frac{q\phi_b}{k_B T}\right)\left[1 - \exp\left(-\frac{qV}{pk_B T}\right)\right]. \tag{12}$$

At low voltage region, i.e., when the applied bias voltage is low, Eq. (12) can be approximated by using the following relationship $\exp(-qV/pk_B T) = (1 - qV/pk_B T)$ and it turns into

$$J = J_0\left(-\frac{q\phi_b}{k_B T}\right)\frac{qV}{pk_B T}. \tag{13}$$

The previous equation means a linear response of J– E or I–V curves at low potential, which is a pattern commonly observed in non-ohmic devices (see Fig. 1 and related discussion on this text).

In general, the above phenomenological description can be applied for specific situations. For instance, considering that the non-ohmic conduction can be explained by thermionic emission enhanced by barrier lowering at low fields with a combination of other mechanisms at high field,[19] Glot have recently, based on an equation which is very similar to the phenomenological Eq.

(13), found interesting results. For the increment of the current density at high voltage it was found that (using the notation of this review):

$$\frac{\mathrm{d}J}{\mathrm{d}V} = -\frac{1}{k_\mathrm{b}T} J(V) \frac{\mathrm{d}\phi_\mathrm{b}}{\mathrm{d}V}, \qquad (14)$$

In a grain-boundary controlled non-ohmic material the current density increment contains two parts. One is due to the increment of electric field at constant conductivity: $\sigma(E)\,\mathrm{d}E = (J/E)\,\mathrm{d}E$. The other reflects the increase on the conductivity due to the barrier height lowering. It can be proportional to the current density and to the increment of electric field (see Eq. (11)). Then the current density increment in non-ohmic material can be written as

$$\mathrm{d}J = -\frac{J}{E}\,\mathrm{d}E + \beta J\,\mathrm{d}E. \qquad (15)$$

Glot integrated Eq. (15) to obtain the semi-empirical equation:

$$J(E) = \sigma_0 E \, \exp \beta E, \qquad (16)$$

where the constant of integration σ_0 is the conductivity of the VDR material at low fields. It was defined that the non-linearity factor is then given by

$$\beta = \frac{\bar{d}}{k_\mathrm{B}T}\left(-\frac{\mathrm{d}\phi_\mathrm{b}}{\mathrm{d}V}\right), \qquad (17)$$

and it is proportional to rate of barrier height with voltage. $\bar{d}$ is the average distance between barrier or average grain size (in the majority of situations), according to the definition given here previously. As expected, at low fields ($\beta E \ll 1$) Ohm's law, i.e., $J = \sigma_0 E$ takes place. At high fields, $\sigma(E) = \sigma_0/E$ is increased with electrical field exponentially: $\sigma(E) = \sigma_0 \exp \beta E$. This semi-empirical model was reasonable applied to different composition of ZnO-based and SnO_2-based VDR's systems.[66,67,68,69]

3. Grain-boundary capacitance in dense polycrystalline semiconductor devices

In polycrystalline semiconductors, the trapping of charge at the grain boundaries has a decisive influence on the electrical transport properties by means of the formation of electrostatic potential barriers.[1,64] It was demonstrated in previous sections that varistor application depends on such electrostatic potential barriers in the interfaces. Furthermore, it will be demonstrated in the following sections that there are others interesting applications which exploit the non-ohmic electrical activity of these interfaces, for instance, as in the case of varistor-type sensors.

When dealing with the grain-boundary properties any model that tries to describe the electrical activity in this region of a polycrystalline semiconductor has to take into account a number of different charges: (i) the electronic interface charge, (ii) the shallow and deep defect screening charges in the bulk and (iii) the minority carrier charge trapped at the interface.

The response of these different charges is determined by a number of parameters such as the density, the energy relative to the valence band edge and the capture cross section and these parameters can be extracted from the steady-state behavior of the grain boundary alone. In this case, a particularly useful experiment, allowing the determination of many parameters, is the admittance spectroscopy (AS).[70,71,24,72] Electronic transitions in semiconductors barrier devices may have the effect of producing longer-range movements of charges. This kind of relaxation can be evaluated in polycrystalline semiconductor by means of AS technique which has been used to the study of Schottky-like barriers, interfacial states and shallow donors or deep trapping levels in polycrystalline ceramics.[70,71,24,72] Here it will be shown how AS can be exploited to obtain relevant information on the grain-boundary electrical properties of semiconductors polycrystalline devices and the attention is focused on the ZnO-based and SnO_2-based devices. However, before this, it is important to present specific and important models dealing with the dielectric behavior of semiconductor junctions which is important to be described, due to the fact they are essential to an understanding of numbers of experimental data described in references mentioned in this section and others at the end of the text.

Many types of semiconductor junctions and devices have been studied making use of this experimental technique. Some examples of this are p–n junctions,[73,74,75] and GaAs Schottky diodes or silicon Zener diodes, all of which have yielded very useful information about the trapping dynamics. In discussing the dielectric properties of barrier regions, it is inappropriate to talk of the *material parameters* such as permittivity $\epsilon(\omega)$ and susceptibility $\chi(\omega)$, since only the complex capacitance $C^*(\omega)$ can be measured because, in most cases, one does *not* have sufficient knowledge of the geometry.[72,74,73] Therefore, results are commonly expressed in terms of the complex capacitance C^* related to the complex susceptibility:

$$\chi^*(\omega) = C^*(\omega) - C_\infty = C'(\omega) - C_\infty - jC''(\omega), \qquad (18)$$

where C^* is the complex capacitance, C_∞ is the limit of C^* at frequencies sufficiently high to render the loss processes of interest negligible.

The equivalent circuit of a Schottky barrier is seen as consisting of three parallel elements: (a) the 'high frequency' limit C_∞ (which, in typical situations, may be above several MHz) of the junction capacitance, at a sufficiently high frequency for all the delayed processes, (b) the complex incremental $C^*(\omega) - C_\infty$ due to delayed processes themselves and, lastly, (c) the conductance, G_0, representing the dc conductance of the barrier.

The dielectric properties of varistor devices were first investigated by Levinson,[25] who found relaxation peaks following Cole–Cole responses with γ values close to 0.2 (it is more common to use α or β to represent the deviation from the Debye response but, in the present context, the α symbol was adopted to represent the non-linear coefficient of the varistor devices and β the non-linear factor). Deep trapping levels in varistor devices have also been characterized by Alim,[24,76] who employed dielectric or admittance spectroscopy to study ZnO-based varistor system. This author observed trapping relaxation behaviors in ZnO varistors at frequencies between 100 kHz and 1 MHz close to room temperature. In addition, a negative termi-

nal capacitance has been reported in this type of system, usually at frequencies exceeding 10^6 Hz.[76,77] This corresponds to an inductive response that produces a resonating effect, commonly modeled by an *LCR* series circuit. In many cases, this resonating behavior to some extent masks the dielectric relaxation response. As indicated by Alim,[78] some samples display three distinct relaxations peaks, but the high frequency one is usually masked by the onset of the resonant phenomenon. Dielectric and admittance spectroscopy have also been used to characterize the nature of the Schottky-type barrier in SnO_2-based varistors.[30,79] Broad loss peaks in ZnO varistor systems have been reported by Garcia-Belmonte et al.[80] Dielectric relaxation models employed for fitting experimental data have also been based on the classic Cole–Cole response, as indicated below:

$$C^*(\omega) = C_\infty + \frac{C_0 - C_\infty}{1 + (j\omega\tau)^{1-\gamma}}, \tag{19}$$

where γ accounts for a distribution of relaxation times and satisfies $0 < \gamma < 1$. The time parameter τ corresponds to the central relaxation time and C_0 represents the low frequency value of the capacitance. It is worth noting that, in this case, the imaginary part of the complex capacitance $C''(\omega)$ consists of a symmetrical relaxation peak that departs from Debye's asymptotic behavior.

In a Debye relaxation process, the high and low frequency slopes of a $\log C''$ versus $\log f$ plot correspond to 1 and -1, respectively. In contrast, a Cole–Cole relaxation response presents slopes equal to $1 - \gamma$ in the low frequency part and $-(1 - \gamma)$ in the high frequency one. This is the most common dielectrical model used for characterizing varistor responses.[81,72,78,79] However, Cole–Cole responses are not the only useful model currently applied in analyzing the dielectric features of ZnO varistors. In this sense, a Havriliak-Negami relaxation function may account for a more general dielectric response.[80,72] As far as asymptotic behavior is concerned, it can be expressed in terms of the 'universal law' function proposed by Jonscher[74]:

$$C'' \propto \left[\left(\frac{\omega}{\omega_p}\right)^{-m} + \left(\frac{\omega}{\omega_p}\right)^{1-n} \right], \tag{20}$$

in which $1 < m < 0$ and $1 < n < 0$. In addition, the m and $-(1 - n)$ power law exponents represent the asymptotic slopes of the relaxation function (for low and high frequency regions, respectively, in a log– log plot) and ω_p is the angular frequency of the loss peak. This type of model is applicable in semiconductor junctions in general and particularly in varistor systems, as pointed out by Li,[82] reporting on a study of degradation effects, and was used by Garcia-Belmonte et al. to characterize trapping in ZnO commercial samples.[80] For SnO_2-based system it is possible to find informations in Refs. 30,64,72,79. The general junction semiconductor theory, based on Debye-like dielectric responses, assures displacements of the loss peak (C'' spectra) when the temperature is raised. The relaxation angular frequency ω_p (or its inverse τ, the time dependence of the electron transition) shows a temperature variation that is well established[79,80,72]:

$$\omega_p = \tau^{-1} = e_n = \sigma_n \nu_{th} N_c \exp\left[\frac{(E_c - E_t)}{kT}\right], \tag{21}$$

where e_n is the characteristic emission rate, σ_n the capture cross-section of the trapping state, ν_{th} the free-electron thermal velocity, N_c represents the conduction band density of states and $E_c - E_t$ is the energy difference between the conduction band and the trapping level. Eq. (21) gives the change in emission rates when varying the measurement temperature. Thus, an estimation of the trapping level energy can be obtained from the following relationship:

$$\ln\left(\frac{\omega_p}{T^2}\right) \propto \frac{1000}{T}, \tag{22}$$

because the product $\nu_{th} N_c$ is proportional to T^2.

It is important to point out that Schottky-type barriers in varistor devices are of the back-to-back type. In other words, they are double Schottky-type barriers. This type of barrier can also be studied based on a voltage dependence of the capacitance.[30,78]

Deep level transient spectroscopy (DLTS) measurements were performed to investigate the effect of Nb_2O_5 and Cr_2O_3 on the electronic states of SnO_2-based varistors.[83] Two electron traps, i.e., 0.30 and 0.69 eV, were identified in both SnO_2· CoO ·Nb_2O_5 and SnO_2· CoO ·Nb_2O_5·Cr_2O_3 varistor's composition. These two traps could be associated with the second ionization energy of oxygen vacancies or impurities on host lattice site. The values found from DLTS spectroscopy are in good agreement with the values found by means of admittance–frequency characteristics[79,72](DLTS and AS are complementary techniques), in which the presence of deep trap states at 0.42 eV in SnO_2· CoO ·Nb_2O_5·Cr_2O_3-based varistor doped with La_2O_3, Pr_2O_3 or CeO_2 where found.[79,72] The results are also in agreement to that found by Orlandi et al.[84] whom subsequently used admittance and dielectric spectroscopy to study SnO_2·MnO-based varistor system doped with Nb_2O_5. They obtained activation energies of about 0.49 eV for the higher frequency loss peaks and about 0.67 eV for the low frequency dispersion. They noted that values obtained for the high frequency process in their studies on SnO_2·MnO-based varistor system, i.e., a anergy value of about 0.49 eV, are comparable with the values found by Bueno et al.,[79] obtained for SnO_2·CoO-based system, i.e., a value of about 0.42 eV.

The energy values around 0.3 and 0.4 eV were attributed to intrinsic atomic defects such as the second ionization of the oxygen vacancy.[83,79] On the other hand, the values found around 0.7 eV is unknown, but could be due to extrinsic defects.[84,83]

To analyze the VDR frequency response behavior it is useful to represent the VDR microstructure by the block model shown in Figs. 2 and 5. This model presumes the device to be assembled of conducting n-type semiconductor metal oxide based matrix (i.e., ZnO, TiO_2 or SnO_2) cubes of size $\bar{d}$ separated from each other by an insulating barrier region of thickness t (see Fig. 5). It is important to be emphasized that the insulating barrier is not a separate phase but is largely a representation of the back-to-back depletion layers at the VDR grain boundaries. However, if inter-

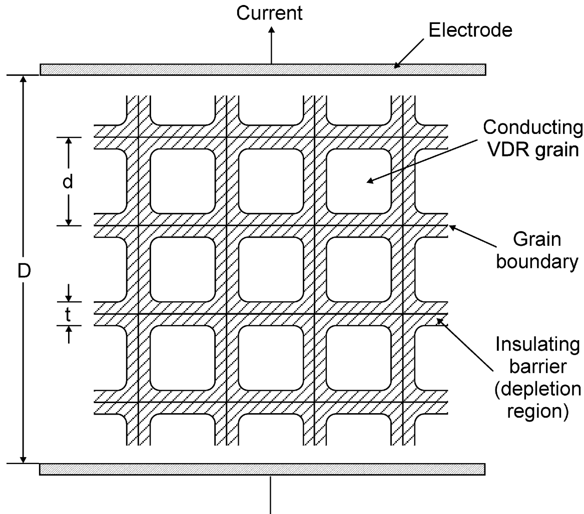

Fig. 5. Schematic representation of the block model of a VDR system possessing a grain size $\bar{d}$ and a separation between electrodes of D. t is the representation of the intergranular depletion layer thickness (better visualized in Fig. 7).

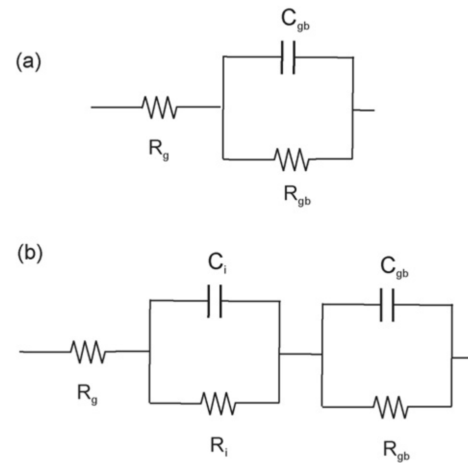

Fig. 6. Traditional equivalent circuit model of a VDR system. For such equivalent circuit representation, the bulk deep trap states are considered to not influence the represented response analysis. R_g is the grain or bulk resistance. R_{cg} and C_{cg} of grain boundary meanwhile the R_i and C_i are respectively the resistance and capacitance of intergranular layer. (a) In this case, the intergranular layer is considered very thin so that its response is ignored, i.e., $R_{gb} \gg R_i$. (b) In this last situation of classical equivalent circuit representation, the intergranular layer is not ignored.

granular layer exist, sometimes the frequency response of the system can present a very different pattern. Indeed, according to the blocking model of Fig. 5, the thickness of insulating dielectric, lying between the sample electrodes, is not D but $Dt/\bar{d}$. Furthermore, since $\bar{d} \gg t$ it is clear that the volume between the varistor electrodes is largely occupied by conducting VDR material (grain). Hence, if k is the dielectric constant of the VDR matrix in the depletion layers, it is expect the VDR capacitance to be given by

$$C = k\varepsilon_0 \frac{A}{Dt/\bar{d}} = \left(\frac{\bar{d}}{t}\right) k\varepsilon_0 \frac{A}{D}, \tag{23}$$

i.e., the effective dielectric constant is increased by a factor of $\bar{d}/t$.

Generally, t has the dimension of the depletion layer.[1] Therefore, it is possible to affirm that the depletion layer largely controls the varistor low-voltage capacitance. The thickness of any intergranular material between the grains in the region of closest grain–grain contact, where the conduction takes place, is at least two orders of magnitude less.[25]

Therefore, in general, the simple equivalent circuit representation of a metal oxide varistor or VDR system is given by a capacitance in parallel with a resistance (see Fig. 6), i.e., the resistance of grain boundary in paralell with its capacitance. The great difference between ZnO- and SnO_2-based varistor system is that for SnO_2, specially if it is doped with CoO (highly dense system), the intergranular layer is very thin, i.e., $R_{gb} \gg R_i$ (see Fig. 6). Note that in Fig. 6 the R_g is the resistance of grain or of the VDR bulk. Usually, this resistance is ignored except for very high currents or at very high varistor frequencies.[16]

In both cases of Fig. 6(a) or (b), bulk deep trap levels are been ignored. However, bulk deep trap levels exist in ZnO-[78,81,80] and SnO_2-based VDR systems,[79,72] influencing the frequency response of the systems (see previous discussion made in this section). Considering the existence of bulk deep trap levels, the equivalent circuit representation becomes that showed in Fig. 7. Actually, depending on the composition or technique employed to investigate the bulk deep trap level, more than one level is possible to be detected in ZnO[81,70,71,80] or SnO_2.[83]

Therefore, to calculate the potential barrier parameters, the grain-boundary capacitance is the only really important capacitance. The separation of grain-boundary capacitance from other capacitances, for instance that related to the deep trap levels, is possible to be done by means of frequency response analysis with a correct equivalent circuit representation of the global response.[72,81] For this purpose, in the majority of situations, the admittance or dielectric representation of the frequency response data is more useful than the impedance representation, specially for very good VDR systems in which the grain-boundary resistance is very high.[72]

Indeed, the calculations of the grain-boundary capacitance are made based on the high frequency intercept associated with high frequency relaxation in the complex capacitance plane,[30,78] which reinforces the need for studying complex capacitance responses.[81,78,79,72] The characteristics of the Schottky-type barrier can be inferred from the applied voltage dependence of the capacitance, which, in the case of varistor systems, owing to the double Schottky-type nature of the barrier, can be sometimes appropriately described using the approach of Mukae et al.,[23,30] which is basically the Eq. (10) written in a different manner, i.e.:

$$\left(\frac{1}{C_{gb}} + \frac{1}{C_{gb,0}}\right)^2 = \frac{2}{qk\epsilon_0 N_d}(\phi_b + V) \tag{24}$$

N_d is the positive space charge density in the depleted region (free electron density). However, in this equation, $C_{gb,0}$ and C_{gb} are the mean value of grain-boundary capacitance per unit area biased, respectively, with 0 and V V. The average number of

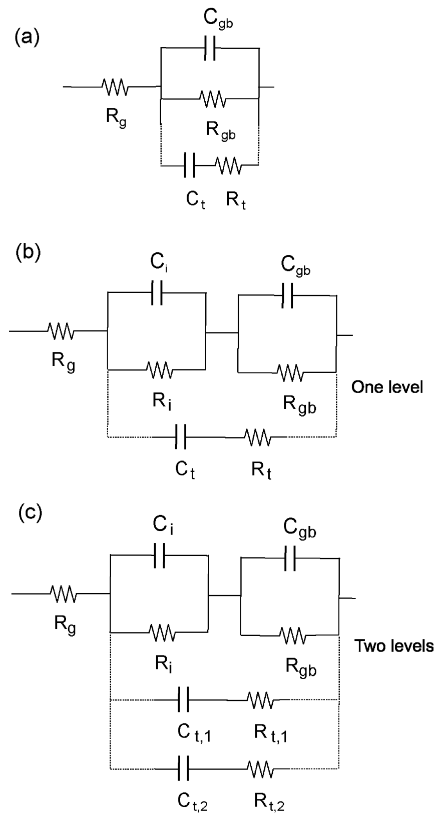

Fig. 7. The most realistic equivalent circuit representation of polycrystalline semiconductor devices must take into account the presence of bulk trap states as schematically represented in this figure. (a) Is the equivalent circuit representation of a VDR devices with very thin intergranular layer (generally the case of SnO_2-based VDR devices) and possessing one significative bulk trap state level. (b) This is the case in which intergranular layer cannot be ignored (observed in some ZnO-based VDR composition). (c) Finally, this is equivalent of case (b), but with two discrete bulk trap state levels.

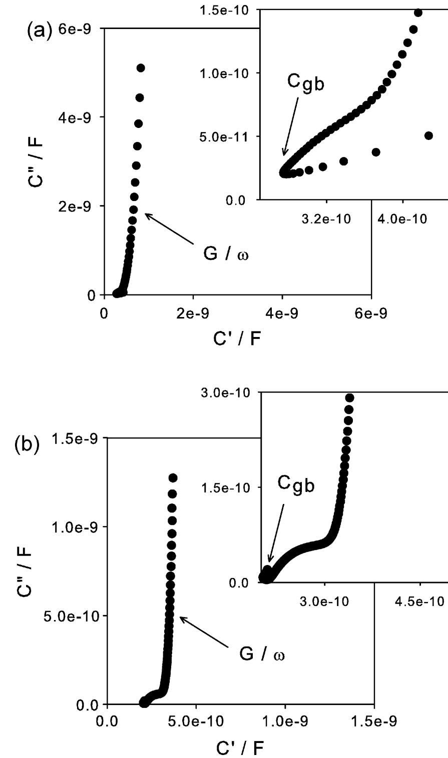

Fig. 8. Complex capacitance behavior of $SnO_2 \cdot CoO$-based varistor system. The response is completely in agreement to the equivalent circuit of Fig. 7(a). In both complex capacitance pattern of case (a) and (b), at low frequency it is observed the term G/ω related to the grain-boundary resistance. At intermediate frequencies, the observed relaxation process related to the deep trap rate dynamics is shown (better visualized in the inset). At high frequency region is where the grain-boundary capacitance can be obtained separated from other capacitive relaxations. The main differences of case (a) and (b) is related to the processing of the VDR devices, showing that the dynamic and occupation of bulk trap states is great influenced by the sintering process and homogeneization of dopants. Finally, note that the bulk trap relaxation is better visualized in case (b).

grains (or barriers) between electrodes is not expressed in Eq. (24).

Oxygen vacancies and electronic defects on the surface of SnO_2 are related[2,4] and have been exhaustively studied.[85,86] Oxygen plays an important role in the grain boundary[2] of ZnO-[4] and $SrTiO_3$-based[5] varistors, since it indicates that the chemistry of the grain boundary determines the electrical nature of this material (nonlinearity between $I-V$ curve). A bismuth film approximately ~ 5 Å thick in $ZnO \cdot Bi_2O_3$-based varistors is required to create potential barriers at the grain boundaries and the height of these barriers is strongly dependent on the excess of oxygen present at the interface between ZnO grains.[4] Similar results were obtained for SnO_2 varistors,[62,64,53] indicating that the formation of a potential barrier is determined by the amount of oxygen present at the interface between grains. Thus, SnO_2- and ZnO-based varistors present similar physicochemical properties.[30] It was proposed[30] that the physical origin of the potential barrier formed in SnO_2 and in ZnO varistors is the same, i.e., that potential barrier have the same origin, both possessing a Schottky-type nature. This aspect was particularly demonstrated using measurements of the capacitance–voltage ($C-V$) characteristics of the system, allied to a complex plane analysis,[79,30] which is basically the methodology detailed described previously in the present section. A significant dispersion of admittance with the ac frequency is typically observed in varistors, giving rise to a complex Mott–Schottky response.[24,78,23] In other words, the grain-boundary capacitance must be determined taking into account the complex capacitance plane. Therefore, the interpretation proposed by Alim et al.[24] is applied in the study of the $C-V$ characteristics of the grain boundary, without incorporating other frequency-dependent phenomena in the analysis. Sometimes, the calculations of grain-boundary capacitance were carried out at the intercept of the high frequency region associated to high relaxation frequencies,[30] see Fig. 8 as an example. The presence of a Schottky-type double potential barrier was observed from the $C-V$ measurements in this region. The dependence of applied grain-boundary capacitance as a function of voltage was obtained using the approximation proposed by Mukae et al.[23] combined at specific frequency, in which the influence of other relaxation processes are minimized and a Mott–Schottky "true" pattern is obtained.[78,72] The density of states at the interface between SnO_2 grains and intergranular layer is estimated by the following

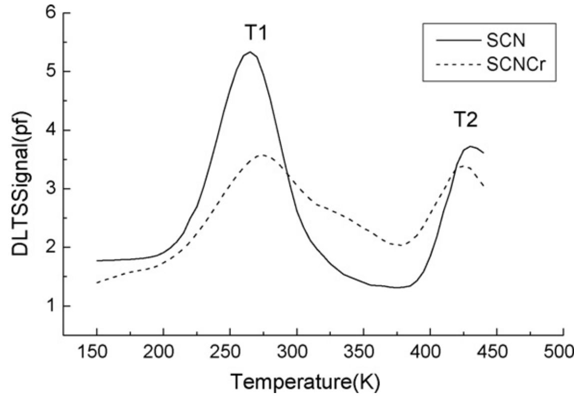

Fig. 9. DLTS spectra for $SnO_2 \cdot CoO$-based system doped with Nb_2O_5(SCN) and $SnO_2 \cdot CoO$-based system doped with Nb_2O_5 and Cr_2O_3 (SCNCr). The spectra shows two energy levels, i.e., around 0.30 and 0.69 eV.[83]

equation (Fig. 9) :

$$N_{IS} = \left(\frac{2N_d k\epsilon_0\phi_b}{q}\right)^{1/2} \quad (25)$$

Grain-boundary capacitance (C_{gb}) is located in the region of transition, while the states trapped at the interface of $SnO_2 \cdot CoO$-based varistors are manifested at lower frequencies, as indicated in Fig. 8. The main conclusion reached by the authors is that, despite the significant difference in the microstructural nature of ZnO and SnO_2varistors, their physical nature is the same and can be described by a Schottky-type double barrier. This Schottky-type barrier is presumed to be associated with the presence of oxygen species at grain boundary in both ZnO and SnO_2.[64,4,92,]Table 1 shows an example of typical values of ϕ_b, N_d and N_{IS} in some SnO_2-based varistor systems, while Fig. 10 presents an example of the C– V characteristics of these systems for different temperatures. Fig. 11 presents the most acceptable model proposed for the potential barrier and the related atomic model that generate the potential barrier formed at grain-boundary region in SnO_2-based varistors. Table 1 also shows the influence of the addition of Nb_2O_5 addition to the $SnO_2 \cdot$ CoO based system. There are an optimal value for the Nb_2O_5 content.[62] After a critical value, the tendency is a decreasing on the non-ohmic properties.[62]

It is possible to observe in Fig. 11 that the transition metal segregated at the grain boundary (illustrated here by Cr precipitate metal, but it could be Cr[61], Co,[13] Pr,[50,87] Dy,[88], Fe[89] Y,[90] Cu[91] or any other transition metal) is the origin of the potential barrier since it is the cause of the formation of an oxide region, i.e., metal oxide region, with a "p-type semiconductor nature"

Table 1
Typical values of ϕ_b, N_d and N_{IS} for double Schottky-type barrier found in $SnO_2 \cdot CoO \cdot Cr_2O_3$-based system doped with different molar concentration of Nb_2O_5.[62]

Nb_2O_5 (mol%)	ϕ_b (eV)	N_d ($\times 10^{23}$ m^{-3})	N_{IS} ($\times 10^{16}$ m^{-2})
0.035	0.73 ±0.05	13.9	3.97
0.050	1.01 ±0.06	4.80	2.75
0.065	0.98 ±0.07	5.09	2.79

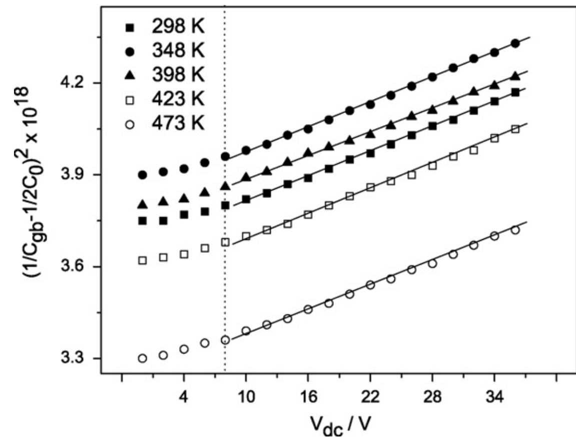

Fig. 10. Mott–Shottky behavior of SnO_2polycrystalline ceramics at different temperatures. From Mott–Schottky behavior is possible to calculate the main physical parameters involved with the electrostatic potential barrier. However, the use of Mott–Schottky curves even when combined with complex capacitance analysis must be carefully used (for more details see Refs. 72,78).

which, in other words, means a metal deficient and oxygen rich region or phase. Therefore, the oxidation of the region depends on the features of the metal oxide segregation and on the thermodynamic equilibrium between oxygen species at grain and grain boundary.[64] Although the model is here illustrated to SnO_2-based system it can be extended to other varistor systems.[64] For example, the studies of Stucki and Greuter[3] have revealed that

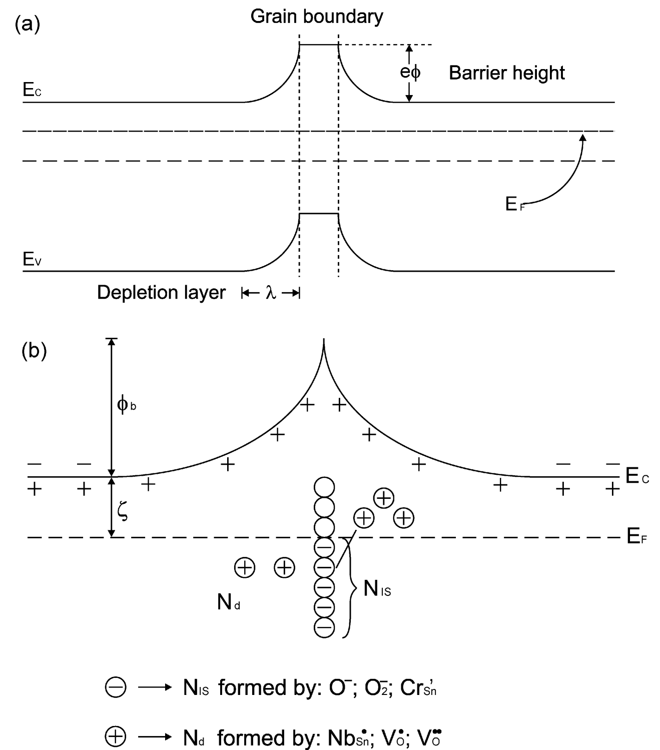

Fig. 11. (a) Potential barrier model of non-ohmic polycrystalline VDR devices. Note that the intergranular layer can be taken into account. (b) Schematic representation of the atomic defect model to the formation of potential barrier in metal-oxide varistor devices (however, as indicated it is specifically described for SnO_2-based VDR systems, specially because the intergranular layer is considered very thin).

the concentrations of oxygen and bismuth at the grain boundaries are affected differently by post-sintering thermal treatment in vacuum and air in ZnO-based varistors. Earlier reports have also suggested that varistor characteristics are related to the particular crystalline form that the Bi_2O_3 takes on[3,65] with oxygen at the grain-boundary surface. Therefore, the grain boundaries can become more oxidized when treated in an O_2-rich atmosphere (because of the ease with its valence state can be changed), causing the electron-trapping interfacial region to become richer in oxygen species, improving the non-ohmic features of these polycrystalline systems.[64,79,62]

More detail of the transition metal segregation was studied recently in ZnO-based varistor system.[87] The role of Pr doping on double Schottky barrier formations at ZnO single grain boundaries was investigated by the combination of current–voltage measurements and atomic-resolution scanning transmission electron microscopy.[87] It was shown that although Pr segregated to specific atomic site along the boundaries, it was found not to be the direct cause of non-linear current–voltage properties. Instead, under appropriate annealing conditions, Pr enhances formations of acceptor-type native defects that are essential for the creation of double Schottky barriers in ZnO.[87]

4. Microstructural comparisons between zinc oxide- and tin dioxide-based polycrystalline compound semiconductors

The metal-oxide varistor are produced by a ceramic sintering process that gives rise to a structure of conductive grains (composed by the matrix oxide) surrounded by electrically insulating barriers (i.e., resistive grain-boundary region). These electrical barriers derive from trap states at the grain-boundaries induced by additive elements.[64,2,117,87]

The milling and homogenization stages of the powders are mainly carried out in a ball mill in an aqueous or alcohol medium. The traditional ZnO-based polycrystalline ceramic is generally densified by the presence of Bi_2O_3, which forms a liquid phase during the sintering stages. Other dopants such as Sb_2O_3, Cr_2O_3, CoO and MnO_2 are added in order to increase the value of α and resistance against degradation.[2] The most appropriate model to describe the non-ohmic properties of ZnO-based ceramics is based on the presence of a potential barrier located at the juncture between grains[1,2] and as commented previously it is similar to that observed in SnO_2-based varistor system.[30] The application of these ceramics as low or high-voltage varistors is directly associated to the number of barriers effectively formed. The potential barrier located in the region of the grain boundary, formed by dopants, depends on the number of defects induced by the dopant atoms segregated in this region. In the case of ZnO-based ceramics, the potential barrier presents a characteristic energy value about 0.8–1.5 eV. The value of barrier voltage per grain lies on 2.6–3.2 V. The nominal voltage of a varistor is proportional to the number of these barriers. Under normal conditions, the average size of ZnO-based varistor grains is about 3–8 μm, a condition that supplies nominal or rupture voltage (E_r) in the order of 1800–8000 V cm^{-1}. For SnO_2-based varistor systems, the values of the barriers also lies between 0.8 and 1.5 eV.[79,93,94,95,55,96]

The non-ohmic behavior of SnO_2-based systems is equivalent to that of the traditional high-voltage ZnO varistors.[30,64] Non-ohmic ZnO-based ceramics have a complex microstructure composed of different crystalline phases such as phases rich in Bi_2O_3, spinel ($Zn_7Sb_2O_{12}$) and pyrochlore ($Zn_2Bi_3Sb_3O_{14}$). The presence of these crystalline phases is easily verified by the use of the X-ray diffraction technique (XRD) and scanning electron microscopy (SEM).[2] In contrast to the ZnO $\cdot Bi_2O_3$-based systems, within the detection limits of the XRD technique, non-ohmic $SnO_2 \cdot CoO$ ceramics present a single phase — the cassiterite (SnO_2) phase. SEM analyses reveal a more homogeneous structure,[61,30,79,53,54,48,97,98,28,13,58,99] as shown in Fig. 12. In the non-ohmic $SnO_2 \cdot$ CoO systems, the CoO forms a solid solution by means of the substitution of Sn^{4+} ions by Co^{2+}or Co^{3+} ions, as described in Refs. 13, 28. These two ions, as shall be discussed later herein, play a determining role in the formation of the potential barrier of non-ohmic $SnO_2 \cdot$ CoO systems. A $CoSnO_3$ phase precipitated in the region of the grain boundary is determined solely by high-resolution electron transmission microscopy (HRTEM)

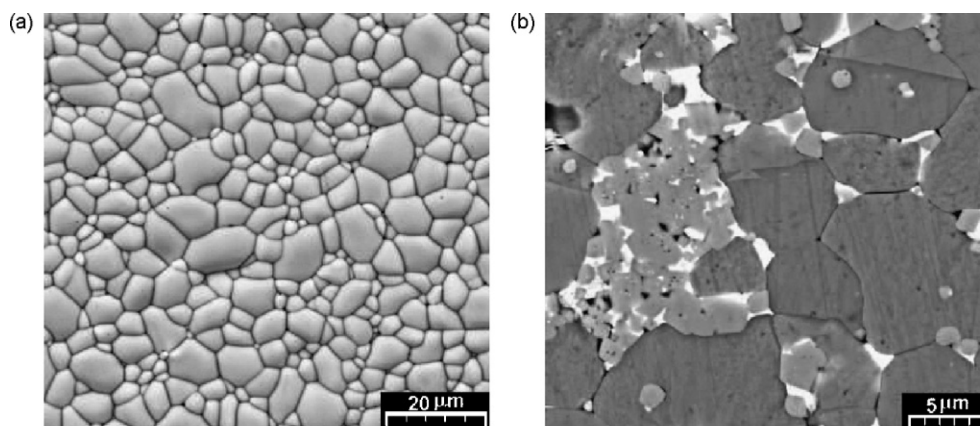

Fig. 12. Comparison between (a) typical microstructure of a SnO_2-based varistor system and (b) ZnO-based varistor system. What is very important to be noted is the influence of the several and different phases in the ZnO-based system. These phases must be carefully controlled during sintering processing. Concerning electrical response, the possibility of the existence of intergranular layer in ZnO-based compositions is most probable than SnO_2(for more details, see discussion on this text).

Table 2
Comparison between basic chemical composition, non-ohmic electrical properties and microstructural features of ZnO- and SnO_2-based varistor systems

Chemical composition (mol%)	T (°C)	d [a] (μm)	Phases	α	E_r (V cm^{-1})
98.9% SnO_2+1.0% CoO +0.05% Nb_2O_5 +0.05% Cr_2O_3	1300	5.4	SnO_2	41	3990
94.9% ZnO+0.5% Bi_2O_3+1.5% Sb_2O_3+1.5% CoO+1.5% MnO_2 +0.1% Cr_2O_3	1250	10.0	ZnO+ β-Bi_2O_3+ α-$Zn_7Sb_2O_{12}$+$Zn_2Bi_3Sb_3O_{14}$	42	2290

Note that the main disadvantage of SnO_2-based varistor system compared to ZnO device is its high sintering temperature. Here the differences is only 50 °C, but sometimes it could reach up to 200 °C.
[a] Mean grain size.

coupled to EDS analyses.[100] The absence of an eutectic liquid suggests that the densification observed in these systems is not associated to liquid phases, but is controlled by solid-state diffusion.[100,]Table 2 presents a comparison between the chemical composition, the electrical properties and the microstructural aspects of SnO_2·CoO and ZnO·Bi_2O_3 varistors. An additional advantage of the SnO_2· CoO over the ZnO·Bi_2O_3 systems is the need for lower concentrations of dopants to obtain equivalent α and E_r values[28,13,58,46,59,60,61,46] allied to greater resistance to degradation.[101] However, the sintering and processing temperature for SnO_2-based varistor system is higher[96,28,46] compared to that found in ZnO-based systems.[2,102,103]

When doped only with CoO, SnO_2 presents a highly resistive behavior and current–voltage linearity up to voltage values in the order of 3000 V. Small molar concentrations of Nb_2O_5 (0.05 mol%) suffice to render the system a varistor with $\alpha\sim 8$ and $E_r = 1870$ V cm^{-1}.[13] This system is generally sinterized at 1300 ° C for 1 h, and then cooled at a rate of 10 °C min^{-1}. A significant increase in the α value of ~ 41 and $E_r = 4000$ V cm^{-1} is possible to be achieved with the addition of 0.05 mol% of Cr_2O_3 to the ternary SnO_2·CoO·Nb_2O_5 system[13] prepared under the same conditions. The addition of greater concentrations of Cr_2O_3, such as 0.10%, 0.30% and 0.50% were also evaluated.[99,61] Additions of Cr_2O_3 in concentrations exceeding 0.05% degrade the non-ohmic properties[61,99] if the above described processing is maintained, mainly due to the fact that the microstructures of these systems depend on the concentration of Cr_2O_3, reducing their density and, consequently, increasing their porosity. This is clearly evidenced when one observes the microstructural evolution of these systems with the addition of Cr_2O_3.[99]

The strong dependence of the microstructure on the addition of Cr_2O_3 suggests that this oxide is present in the region of the grain boundary, which can make densification difficult but which can, in small concentrations, contribute significantly to increasing the non-linear coefficient values. An increase of the sintering temperature from 1300 to 1350 °C, maintaining the same 1-h sintering time, suffices to increase the system's homogeneity and density by using 0.1 mol% of Cr_2O_3, producing a system with $\alpha\sim 29$ and $E_r = 6807$ V cm^{-1}, but is insufficient to produce non-ohmic ceramics with Cr_2O_3 concentrations in excess of this value. Thus, Cr_2O_3 plays two fundamental roles: (a) in small concentrations, it increases the α and E_r values, and (b) in large concentrations, it gives rise to porous microstructures that lead to highly resistive ceramic materials. Studies of these systems by impedance spectroscopy carried out by Bueno et al.[61] suggest that the addition of Cr_2O_3 not only increases the system's porosity but also its presence in the grain boundary increases the potential barrier values and density of states trapped in the grain boundary. Hence, if present in large concentrations,[61] it may give rise to a system with very high values of dc resistance without non-ohmic behavior up to values of 10,000 V cm^{-1}.

Antunes et al.[60] demonstrated that Ta_2O_5 plays the same role as Nb_2O_5 in the SnO_2·CoO-based system when substituted in the same concentration, without substantially altering the α and E_r values. This strongly suggests that the importance of this additive lies in its valence state (5+),[60,49] contributing to increased electronic conductivity (see Eq. (26)) inside the SnO_2 grain:

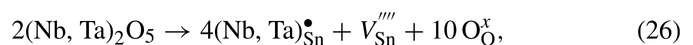

$$2(\mathrm{Nb, Ta})_2\mathrm{O}_5 \rightarrow 4(\mathrm{Nb, Ta})^{\bullet}_{\mathrm{Sn}} + V''''_{\mathrm{Sn}} + 10\,\mathrm{O}^{x}_{\mathrm{O}}, \quad (26)$$

$$V''''_{\mathrm{Sn}} \rightarrow V^{x}_{\mathrm{Sn}} + 4\mathrm{e}'. \quad (27)$$

Additions of Bi_2O_3 in the SnO_2·CoO·Nb_2O_5 systems lead to increased grain size and reduced E_r [51,58]; however, they do not significantly augment the α values, which remain at levels of ∼10, similar to the SnO_2·CoO·Nb_2O_5 system, without the presence of Bi_2O_3.[58] The study of the influence of processing on SnO_2·CoO systems began with the work of Leite et al.,[105] who found that non-ohmic properties are strongly dependent on the cooling rate during sintering. Increasing the cooling rates reduces the α values, while slow cooling causes a significantly increasing in these values. The SnO_2·CoO·Nb_2O_5 system, for instance, sintered at 1300 ° C for 2 h, using a 2 °C.min^{-1} cooling rate, presented $\alpha\sim 28$ and $E_r = 5300$ V cm^{-1}. This is a fairly high value for a ternary system owing to the presence of small amount of dopants, particularly in comparison to the traditional multicomponent ZnO systems.

5. The effect of annealing at oxidizing and reducing atmospheres and microstructure heterogeneity

The study carried out by Leite et al.[46] also revealed the effect of the thermal treatment in oxidizing and reducing atmospheres on the non-ohmic properties. An oxidant atmosphere (rich in O_2) can raise the value of $\alpha\sim 28$ ($E_r = 5300$ V cm^{-1}) to $\alpha\sim 32$ ($E_r = 6100$ V cm^{-1}). However, really marked alterations are observed in these systems when the material is thermally treated in a reducing atmosphere (rich in N_2); under such conditions, values of $\alpha\sim 1.5$ are obtained.

The influence of the thermal treatment after sintering was also studied by Cassia-Santos et al.,[62] who found that this α value reduction effect caused by thermal treatment in a N_2-rich atmo-

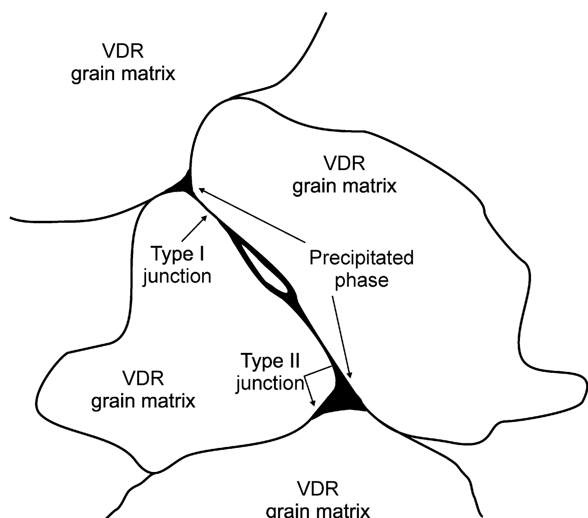

Fig. 13. Example of the reversibility of non-linear coefficient of $SnO_2{\cdot}CoO$-based polycrystalline ceramics after thermal treatments in oxidizing and reducing atmospheres.

sphere is reversible in the majority of situations, as illustrated in Fig. 13. The effects of the cooling rate and sintering temperature were also studied by Oliveira et al.,[50] who confirmed the tendency of α to increase with reduced cooling rates. These authors also evaluated the effect of the addition of La_2O_3 on the non-linear properties of the ternary $SnO_2{\cdot}$ CoO $\cdot Nb_2O_5$ system, concluding that this system's non-ohmic properties are sensitive to small concentrations of both La_2O_3 and Cr_2O_3, which is in agreement with the aforementioned studies of Pianaro et al.[13] and Bueno et al.[61] Thus, the action of La_2O_3 on the material is apparently the same as that of Cr_2O_3, affecting the potential barrier in the region of the grain boundary. The influence of the cooling rate on the varistor properties of SnO_2-based systems is attributed to the oxidizing effect of CoO during cooling (in general, not only the CoO can be oxidizing, but all transition metal segregated to grain-boundary region) and change in the valence state of CoO, as shown in Eq.(28)–(30):

At 600 °C:

$$2CoO + 1/2O_2 \rightarrow Co_2O_3. \qquad (28)$$

At 800 °C:

$$Co_2O_3 + CoO \rightarrow Co_3O_4. \qquad (29)$$

At 1000 °C:

$$Co_3O_4 + CoO \rightarrow 4CoO + 1/2O_2. \qquad (30)$$

According to the above equations, therefore, CoO oxide may affect the states trapped in the grain boundary and modify the potential barrier. The above-described mechanism may give rise to a grain boundary richer in O_2 species caused by less coordinated oxygen than that present in the lattice. Some of the species suggested are ${O_2}^-$, O^- and O^{2-}, which, as is known, are responsible for the formation of non-ohmic properties in porous polycrystalline SnO_2 ceramics used as sensors.[135] Assuming that the origin of the potential barrier is related to these species, it is clear that a reduced cooling rate would increase the density of trapped states in the grain boundary and, hence, the α and E_r values. There are evidences in the literature indicating that the chemistry of the grain boundary in non-ohmic ceramic materials is similar independent of the metal oxide matrix, mainly in regard to the presence of oxygen.[61,85,86,4,92,5,105] The evidences of the presence of oxygen species (which generate trapped states) on the surface of the grain boundary may lead to a reasonable physicochemical model to explain the non-ohmic property of SnO_2 oxide,[42] ZnO,[4,92] and $SrTiO_3$.[5]

It is important also to emphasizes that the SnO_2were already tested as dopant in ZnO-based polycrystalline systems.[27,55] The ZnO-based varistor composition was systematically substituted with SnO_2 in the range from 0% to 100%. The microstructural characteristics, average grain size and the general phase composition were not influenced by the substitution of ZnO by SnO_2. In all the samples it was observed ZnO, Bi_2O_3-rich and spinel phases, where the composition of the spinel depends on the Sb_2O_3 to SnO_2 ratio in the starting composition. The SnO_2 do not influence the non-ohmic behavior but the leakage current were shown to increase. Besides, SnO_2 shows a strong donor effect in the ZnO polycrystalline non-ohmic ceramics.[107] Daneu et al.[56] demonstrated that it is possible to form inversion boundaries when SnO_2 is added to ZnO–Bi_2O_3 which cause anisotropic grain growth in the early stages of sintering and ZnO grains that include inversion boundaries grow exaggeratedly. It can also be observed the presence of a secondary phase for higher amounts of SnO_2. Fayat et al.[108] argued that addition of dopants such as Co_3O_4, ZnO, MnO_2, Sb_2O_3 stabilize valences such as Co^{2+}, Zn^{2+} and Mn^{2+} in the lattice. Specially Sb_2O_3 and Nb_2O_5 reduces the grain growth.[109] The heterogeneity cause by secondary phase was also evaluated by Parra et al.[110] The role of oxygen vacancies on the microstructure development was also evaluated by Parra et al.[111]

Although the dense $SnO_2{\cdot}$ CoO systems, which have been the systems most exhaustively studied for varistor applications,[28,62,30,64,79] display highly non-linear coefficient values (α), when small amounts of other oxides are added, whose metals stabilize in valences of 5+ and 3+, e.g., Nb_2O_5 and Cr_2O_3, respectively, other systems, such as $SnO_2{\cdot}$ ZnO and $SnO_2{\cdot}$MnO, have also been studied for non-ohmic devices applications.[33?,104,113,109,84,114] Therefore, when MnO is applied as a densifying agent of SnO_2 matrix different non-ohmic features arise, possibly due to the sintering mechanisms and densification rate, which are different in $SnO_2{\cdot}$MnO-based polycrystalline ceramics.[109,84] Doping SnO_2 with MnO or CoO leads to the creation of additional oxygen vacancies, which in turn increases the diffusion rate of oxygen ions, altering the sintering of SnO_2 polycrystals. However, the microstructure of $SnO_2{\cdot}$CoO-based ceramics is more homogeneous than the microstructure of $SnO_2{\cdot}$MnO, in which the presence of precipitate phase, mainly at triple points of the grain boundary, is easily visible.[109,84] Therefore, the solubility of Mn^{2+} atoms in the SnO_2 matrix appears to be lower than that of Co^{2+} in the SnO_2 matrix. Reports have mentioned the formation of Mn_2SnO_4 and $MnSnO_3$ in the grain-boundary region.[32,100]

The influence of the distribution of transition metal oxide along the grain boundary appear to be very important in any

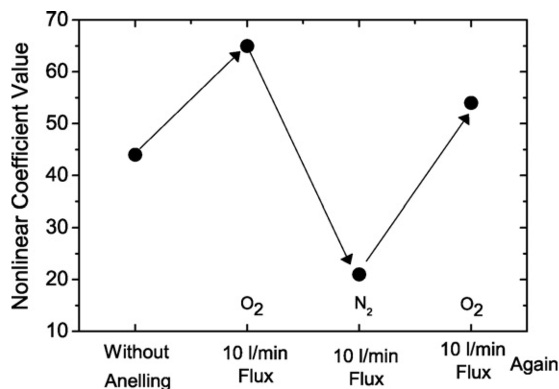

Fig. 14. Schematic representation of the most common heterogeneities found in SnO_2-based varistor system. For instance, for a SnO_2·MnO-based system which is much more heterogeneous compared to SnO_2·CoO-based system, it is possible to observe two types of junction, i.e., type I and II junctions. Type I is thin and Mn-rich while type II junctions are thicker and Mn-poor.[84] The excess of dopants generally generates precipitates at triple point. These precipitates are sources of heterogeneity and capable of degree homogeneity. This effect have great consequences for electrical properties.[116]

kind of varistor-type device. For instance, the additives on the electrical potential barrier at grain boundaries in a ZnO-based multilayered chip varistor was investigated recently.[115] The additives distribution was analyzed by scanning surface potential microscopy and transmission electron microscope. The leakage current strongly depended on the distribution of additives, and a more uniform distribution improved the electrical nonlinearity.[115]

The degree of microstructural heterogeneity in ZnO–Bi_2O_3-based varistors is capable to affect the non-ohmic properties as observed by Li et al.[9]

As pointed out in Ref. 116, when precipitates are present in higher concentrations at triple points they can affect the nature of SnO_2–SnO_2junctions, and hence, the number of active barriers (see Fig. 14). Once these precipitates are present in triple junctions of the microstructure, they can cause adjacent SnO_2–SnO_2junctions poor in segregated metal atoms because precipitates consume the segregated metal atoms in regions adjacent to them. Such adjacent regions generate junctions that will present non-effective potential barriers, so that a parallel conduction through these non-active barriers will occur in varistor devices.[116] This parallel conduction is responsible for an increase of leakage current, which can prevent the non-ohmic properties from being improved. Sometimes, thermal treatments in oxygen-rich atmospheres do not increase the potential barrier and density of states at the interface because the oxygen species are consumed preferentially to eliminate the non-active potential barrier in regions with lower concentrations of segregated metal, thus enriching the precipitates with oxygen species.[116,109,84]

It is important to elucidate here the differences between segregated metals and precipitated phases. Here it is considered precipitated phases the regions in the microstructure (in the present case, the triple points region) which has a well-defined crystalline structure differing from that of the exhibited by the matrix. The region of segregated atoms at the grain boundary has no proper crystalline structure, but it shares the structure of the grain boundary. Segregated metals can sometimes originate an intergranular precipitated phase and sometimes the coexistance between two forms of crystalline structure is not possible to be completely separated. Therefore, in the case of the SnO_2· MnO polycrystalline system, there are two types of junctions, which have different concentrations of segregated metal.[109,84] In this kind of system it was identified different amounts of precipitated phase at triple points of the grain boundary, depending on the doping concentration of Nb_2O_5 and/or sintering time employed during the synthesis of the devices. An extensive intergranular layer of precipitated phase is not observed in the SnO_2· MnO compositions,[109] although precipitates phase at grain-boundary triple points is very common[109] to be observed by SEM analysis.

According to what was discussed in the last paragraph, the non-ohmic properties are controlled by the distribution of type I and II junctions. Type I junctions favor the non-ohmic behavior of SnO_2· MnO polycrystalline ceramics, while type II junctions do not.[109,84] Moreover, type II junctions are responsible for increasing the leakage current of the materials (see Tables 1–3 of Ref. 109). These junctions are also associated with the amount of precipitated phase at triple points of the grain boundary, in as much as they impoverish adjacent junctions, activating the Mn transport in this type of junction, thus forming type II junctions. On the other hand, inducing the precipitation of Mn_2SnO_4phase also causes the increased formation of type II junctions, in detriment to the non-ohmic properties.[109,84] This observation is congruent with what was discussed in Refs. 116,109.

The influence of $Nb_2O_5$was also evaluated in the SnO_2· MnO polycrystalline ceramics and related to the type of junctions.[84] It was shown that Nb_2O_5-doping increases the systems' non-ohmic properties because it increases the fraction of type I junctions, hindering the sintering process and the precipitation of Mn_2SnO_4 phase (it increases the homogeneity of type I junctions). In contrast, longer sintering times decrease the non-ohmic properties because an increasing of the sintering time leads to greater Mn diffusivity, larger amounts of precipitated Mn_2SnO_4 phase, so that the presence of type II junctions in greater amounts cause microstructural heterogeneity, resulting in a deleterious effect on the system's non-ohmic features.[109,84]

It can be concluded, in general, that Nb-doping causes the non-ohmic properties to increase due to the fact that this dopant contributes to hinder the sintering process, increasing the homogeneity of junctions. On the other hand, longer sintering times increase the precipitation of $Mn_2SnO_4$and the heterogeneity of junctions.[109,84]

The most specific and significant conclusions concerning the studies made on SnO_2· MnO binary systems are: (i) the SnO_2· MnO system consists of two phases, SnO_2grains and Mn_2SnO_4, precipitated along multiple grain junctions. (ii) Two types of SnO_2–SnO_2 grain boundaries were identified: type I – thin and rich in Mn and type II – thick and poor in Mn. (iii) Changes in the concentration of Mn along the grain boundary are associated not only to grain misorientation but also to Mn diffusivity along the grain boundary, which controls the junctions' heterogeneities.[109,84]

An analysis of the admittance and dielectric response of SnO_2·MnO-based varistors in the frequency range of 100 Hz

to 15 MHz and a temperature range of 293–573 K allowed the formation of electronic transitions in space-charge regions to be characterized as a function of the Nb_2O_5dopant concentration in SnO_2· MnO polycrystalline-based ceramics.[84] This analysis revealed that the formation of trapping states in space-charge regions was indirectly dependent on the concentration of Nb_2O_5 as a result of a microstructural modification, as discussed in Refs. 84,109. Moreover, the presence of type I SnO_2–SnO_2grain boundaries, which are thin and Mn-rich, was found to favor the formation of space-charge regions in this kind of device. In the systems under consideration, oxygen vacancies or $Mn_{Sn}{}'$-like defects were suggested as the source of trap states situated around of energy value of ∼0.49 eV below the conduction band.[84] The samples were also found to display very dissimilar dielectric responses in terms of the power law exponents of the peak loss, which were attributed to the influence of the conductance term of type-II junctions whose frequency cannot be separated from the trapping relaxation process. As a result, Mott–Schottky plots could not be constructed for the SnO_2·MnO-based systems studied as discussed in Ref. 84.

Generally, it is believed that in the case of ZnO-based varistor system, the non-ohmic properties is closely related to the grain-boundary atomic structures. As different grain boundaries have different atomic structure, different grain boundaries have different influence on the properties. This aspect was studied in details by Sato et al.[117] The relationships between the atomic structures and the electrical properties were investigated using ZnO bicrystals, whose grain-boundary orientation relationship and grain-boundary planes can be arbitrarily controlled. It is considered that the coordination and bond lengths of atoms in the grain boundaries differ from those in the bulk crystal, this does apparently not generate deep unoccupied states in the band gap. This indicates that atomic structures of undoped ZnO grain boundaries are not responsible for the non-linear I– V characteristics of ZnO ceramics.[117] On the other hand, the non-linear I–V characteristic appeared when the boundaries were doped with Pr. High-angle annular dark-field scanning transmission electron microscopy (HAADF-STEM) image of Pr-doped boundaries revealed that Pr segregates to specific atomic columns, substituting Zn at the boundary.[117] However, the Pr itself was not the direct origin of the non-linear I– V characteristics, as the Pr existed in the three-plus state and would not produce acceptor states in the boundary. First-principles calculations revealed that Pr doping instead promotes the formations of acceptor-like native defects, such as Zn vacancies.[117] It is believed that such acceptor-like native defects are microscopically the origin of the non-linear I– V characteristics. Investigations of various types of grain boundaries in the Pr- and Co-doped ZnO bicrystals indicated that the amounts of Pr segregation and the non-linear I– V characteristics significantly depend on the grain-boundary orientation relationship.[117] Larger amount of Pr segregation can cause higher nonlinearity in I– V characteristics, which is mainly obtained for incoherent boundaries. This indicates that Pr doping to incoherent boundaries is one of the guidelines to design the single grain boundaries with highly non-linear I– V characteristics. All of the results obtained by Sato et al.[117] is in agreement to the model proposed in Ref. 64 since Zn vacancies can be caused by oxygen enrichment of the grain boundary induced by p-type metal oxide segregation. Finally, a Pr and Co-doped bicrystal with an incoherent boundary was fabricated to demonstrate a highly non-linear I– V characteristic. This result indicates that ZnO single-grain-boundary varistors can be designed by controlling grain-boundary atomic structures and fabrication processes.[117,64]

Still concerning homogeneity and grain-boundary structures of SnO_2-based varistor system, based on the EFM (electrostatic force microscopy) images, it was proved the homogeneity of the SnO_2· CoO system and the percentage of effective barriers was calculated using the following relationship $\%n_e = 100(n_e/n_t)$ in SnO_2·CoO-based varistor system. The $\%n_e$ is the percentage of effective potential barrier, n_e is the number of effective or active potential barrier and n_t is the total number of barriers. It was shown that 85% of the grain-to-grain junctions in the SnO_2·CoO-based system were active potential barriers. At this point, it is important to point out that this value is higher than that reported for ZnO-based varistors, which is generally considered to range from 15% to 33%.[118,119] As Fig. 15 shows, the charge density varied as a function of bias voltage applied between the tip and the surface of the SnO_2·CoO-based sample. At higher negative or positive voltages, the charge density was higher and its value decreased as the bias voltage decreased, reaching a minimum value in the range of 1–2 V, which is consistent with the presence of Schottky potential barriers.

The value calculated for potential barrier height was shown to be comparable to the values obtained through the conventional use of Eq. (10) combined with a complex capacitance analysis.[78,79,72] The potential barrier height obtained by EFM analysis was about 1.4 eV and the value found by means of the conventional methodology, i.e., by combining Eq. (10) with complex capacitance analysis, i.e., considering the block model, was about 1.3 eV.[120] The values obtained by these two different methodologies were found to be in good agreement and this agreement was specially explained considering the high amount of potential barrier founded in the SnO_2·CoO-based sample (which facilitates the analysis)[72] allied to its simple microstructure in which the morphology of the grains are very uniform (see Fig. 15). Note that for such calculation, the value of the p, i.e., the number of barrier between electrodes was corrected considering the number of active barriers.[120] It is also important to emphasize that, for the calculation of the barrier height by means of complex impedance analysis, the p parameter was corrected by considering the value of $\%n_e$, calculated from EFM. The total amount of active barrier was calculated as about 85% of total potential barriers. Therefore, the p was considered $p = 0.85D/\bar{d}$.[120] More details of the influence of the p parameter on the use of $C - V$ analysis is discussed in [72] Ref. 72. The value of 85% of active potential barriers must be the origin of the better correlation obtained between barrier height values and non-ohmic properties in metal oxide SnO_2-based system (85%) compared with metal oxide ZnO-based varistors (15–35%).[72] The larger number of active potential barriers in SnO_2 metal oxide based VDR systems is possibly related to the difficulty in obtaining low voltage varistors in SnO_2 polycrystalline systems.[120]

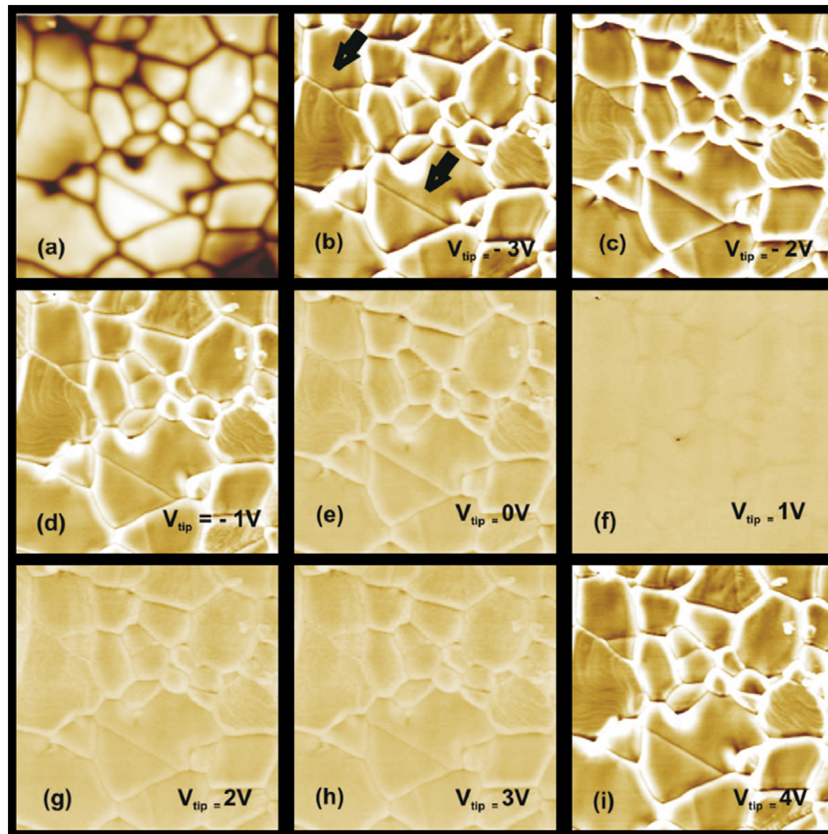

Fig. 15. (a) Here it is shown a typical AFM (height mode) image of the varistor morphology and (b)–(i) shows the EFM images (frequency mode)as function of applied bias voltage. The EFM images indicate that increasing the bias tip voltage (with positive or negative signal) caused an increase in the negative charges stored in the GB region. The charge accumulation observed in the grain-boundary region indicates the presence of active potential barriers or active grain junctions. Furthermore, it is important to stress the existence of inactive junctions, as indicated by the black arrows in (b).

As SnO_2, TiO_2as matrix can also be design to surge arrester applications, possessing non-ohmic behavior without the needs of a densifying agents because TiO_2 is easier densified as already discussed previously. Yan and Rhodes first reported that (Nb, Ba)-doped TiO_2 ceramics have an useful varistor properties[7] to be used as low voltage surge arresters, with a low non-linearity coefficient of ($\alpha\sim$ 3–4), with an oxidizing atmosphere during cooling necessary to achieve better results. The effect of oxidizing atmosphere on the electrical properties of TiO_2 doped with a small quantity of Al was investigated by Pennewiss and Hoffmann.[8] The best non-linear coefficient ($\alpha\sim$ 7) was obtained when the voltage-dependent resistivity was caused by opposite surface oxidation layers of the pellets, rather than grain-boundary effects within the pellets. The processing of a single phase TiO_2 doped with the same concentration of Cr_2O_3 and Nb_2O_5 found in highly non-ohmic $SnO_2{\cdot}CoO$-based polycrystalline system is also capable of activate non-ohmic behavior in TiO_2 according to Ref. 43. The addition of Nb_2O_5in small amounts to the TiO_2or SnO_2 ceramics leads to an increase of the electronic conductivity in the TiO_2/SnO_2 lattice, due to substitution of Ti^{4+}/Sn^{4+} by Nb^{5+}, equivalent to the solid state reaction presented in Eq. (26).

However, due to the grain growth in TiO_2 polycrystalline ceramics, the varistor has a low breakdown voltage, which is desirable to applications as low voltage surge arresters.[112,121,122,123,124,125,126,127] In analogy, it was demonstrated that similar description can be given in (Sn_x, Ti_{1-x})O_2-based systems. Therefore, $(Sn_xTi_{1-x})O_2$ semicondutor polycrystalline structure are promising materials to be used also as varistor devices,[53,54] offering an enormous range of opportunities based on the control of grain-boundary characteristics and of barrier layers. At this point it is important to mention a little more about (Sn, Ti)O_2 systems as ceramic matrix.

6. Tin dioxide- and titanium dioxide-based polycrystalline semiconductor

In this section it will be discussed deeply on the design of electronic devices based on polycrystalline semicondutor ceramics of SnO_2, TiO_2 and $(Sn_xTi_{1-x})O_2$ solid solution rutile-type structure. Therefore, it is important to emphasizes that like SnO_2, TiO_2 in the rutile phase is an electrically semiconductive ceramic (as well as an n-type semiconductor) material with a tetragonal crystalline structure. The electronic gap difference of stoichiometric SnO_2 ($\sim$ 3.6 eV) from that also stoichiometric TiO_2 ($\sim$ 3.2 eV) is around 0.4 eV. Despite of the rutile crystalline structure and band gap, there are other similarities between SnO_2 and TiO_2 solid oxides. The Ti^{4+} ion has an ionic radius value of 0.68 Åwhile, in Sn^{4+}, the ionic radius value is 0.71 Å. Therefore,

the substitution of Sn^{4+} by Ti^{4+} (or Ti^{4+} by Sn^{4+}) in the binary system lattice is expected to not generate oxygen vacancies or another kind of solid state point defect.

TiO_2 and SnO_2 are applied as sensor or varistors and some kind of sensor properties are either based on the grain-boundary potential barrier. In other words, in both applications (sensor or varistor) there are similarities involved in the control of the sensor and varistor properties, which can mainly ascribed to the grain-boundary structure and composition.[135,128] The similarities found are consistently explained by the fact that all of these n-type semicondutor ceramics have the tendency to establish a grain-boundary region with a "p-type semiconductor nature" (due to metal transition atoms segregated at the grain-boundary region and then favors negative charged species to adsorbates and enriches this region). This configuration enables electrons to become localized on the surfaces, giving rise to a negative surface and, as a result, electron depletion layers are formed, acting as potential barriers which control the properties of the mentioned devices. Pure or doped TiO_2, for instance as thin film configuration, can be used for their optical behavior or for some interactive combination of particular properties and behaviors.[129]

It was demonstrated that similar description of that related to SnO_2-based system can be given in $(Sn_x, Ti_{1-x})O_2$-based systems. A matrix founded on $(Sn_x, Ti_{1-x})O_2$-based systems doped with Nb_2O_5leads to a low voltage-based varistor system with non-linear coefficient values of approximately 9.[54,53] The presence of the back-to-back Schottky-type barrier is observed based on the voltage dependence of the capacitance. When doped with CoO, the $(Sn_x, Ti_{1-x})O_2$-based system presents higher non-linear coefficient values ($\alpha > 30$) which is comparable to the values found in SnO_2-based varistor system.[53] Therefore, it can be inferred that Co atoms act as an oxidant agent in the grain-boundary region increasing the barrier height and non-ohmic properties.[53] However, in this situation, the grain growth decreases and breakdown voltage greatly increases. In $(Sn_x, Ti_{1-x})O_2$-based systems there is the advantage of controlling the Ti atoms content so that the microstructure can be designed as desired. Therefore, this varistor matrix may give rise to low or high voltage varistor applications, depending on the composition of the matrix and the nature of the dopant.[53,54] The non-ohmic properties of this system derive from the presence of Nb_2O_5, which is probably responsible for the grain (bulk) conductivity, analogous to that of the SnO_2-based varistor system. The presence of Schottky-like barriers was inferred from capacitance–voltage characteristics. These Schottky-like barriers are ascribed to the presence of a thin precipitated phase (and/or segregate thin layer) in the grain-boundary region and relate to the typical spinodal decomposition frequently observed in these $(Sn, Ti)O_2$ systems.[54] The SnO_2–TiO_2 system possesses a nearly symmetric miscibility gap.[54]

Upon cooling a solid solution from a high temperature in the miscibility gap, a structure consisting of finely divided lamellae alternatively rich in Sn and Ti, is formed within each polycrystalline grain.[54] Therefore, there are several processing variables to be exploited to design different properties of $(Sn, Ti)O_2$ systems. Particularly in gas sensor applications,[130,129] Radecka et al.[129] have studied the SnO_2-TiO_2 compositions[130] and have explored the transport properties[129] of polycrystalline ceramics and thin films. However, apart from this, little is known about the basic electrical features of the $(Sn, Ti)O_2$ system and the answers to questions regarding mass transport, charge carriers and the sintering mechanism have not yet been addressed in detail. Some sintering studies are given in [54] Ref. 54 where the authors investigate the sintering parameters and some aspects of mass transport in $(Sn, Ti)O_2$polycrystalline ceramics with different compositions prepared by a mechanical mixture of oxides, correlating them to the chemical bonding nature and to intrinsic structural defects of these polycrystalline ceramics. The increasing amounts of TiO_2 cause an increase on the density and sintering rate.[54] The TiO_2 concentration on the solid state $(Sn, Ti)O_2$ composition also are responsible for the higher mean grain size value in the composites.[54]

7. Similarities between metal oxide dense varistor and varistor-type sensor

When fully dense, SnO_2display properties similar to those observed in TiO_2 for low voltage varistors[6] and humidity sensors,[39] as already commented previously. However, the behavior of TiO_2 and SnO_2 differ greatly at high temperatures so that TiO_2 differs from SnO_2 during sintering because, unlike SnO_2, no dopants are required to densify it. Densities close to the theoretical[6] values are achieved by sintering at around 1300 °C. The higher porosity and less densified microstructure observed for SnO_2 polycrystalline ceramics is consequence of nondensifying mass transport mechanism achieved during the sintering of the material (see Fig. 3, for instance, regarding differences between dense microstructure and porous microstructure of SnO_2polycrystalline semiconductor). The electrical properties of low density SnO_2polycrystalline ceramics depend on the non-stoichiometry of the oxide surface, the powder preparation methodology, the temperature, and atmosphere used during thermal treatment. This dependence on non-stoichiometry is related to poor densification, which was already discussed in the introduction. An important feature of the highly porous SnO_2-based electronic ceramic devices is related to the existence of negatively charged oxygen adsorbates, such as O^-, O^{2-}, etc., on the surface of SnO_2 grain boundaries (and/or particles). This feature is known to play an important role in detecting inflammable gases.[34,131,135,128] For this reason, oxygen vacancies and electronic states on SnO_2 surfaces have been studied in great detail.[34,131,135,128] The most commonly accepted model for the operation of an n-type semiconductor gas sensor is based on the variation in the potential barrier height at the grain boundary, induced by the change in the amount of oxygen adsorbates by reaction with inflammable gases. However, non-linear I–V characteristics in SnO_2 porous ceramics are observed only at temperatures above 250 °C, because oxygen adsorbates are favored and form a Schottky-like barrier between grains at temperatures exceeding 250 °C.[135] Highly porous SnO_2-based electronic ceramic are used also as solid-state NO_x sensors. Nitrogen oxides (mainly NO and NO_2) are produced in combus-

tion furnaces and automobile engines, and are typical pollutants causing acid rain and photochemical smog. For effective control of both, the combustion conditions and the NO_x-eliminating systems, high performance porous SnO_2 chemical sensor have been developed.[135,128] The SnO_2 chemical sensor mechanism based on chemisorption of oxidizing gases such as NO_x competes with the traditional solid state electrolyte such as stabilized ZrO_2 equipped with oxide electrodes.

It is important to emphasize that dense ZrO_2 is mainly applied as a bulk-type sensor material for pollutant gases such as NO_x or O_2, contrary to the SnO_2 or TiO_2 that is mainly used as thin-type sensor material. Both kind of devices are oxygen sensors, but the first one operates in a different mechanism based on Nernst effect, where an electrical potential is created in an oxygen pressure gradient. In the resistive oxygen sensors based on TiO_2, a peace of TiO_2 dense ceramic material operates at the same temperature as a porous sensor of TiO_2. This is necessary to compensate the temperature-dependent effect. As the TiO_2 dense ceramics does not equilibrate quickly with the gas stream, a reference point to the conductivity can be established.[132] This is not necessary to oxygen sensor that operates based on Nernst effect. In addition, SnO_2 porous semiconductor ceramic is been largely studied to be applied as sensor device in a new category of gas-sensor namely varistor-type gas sensor.[135,128] Traditional semiconductor gas sensors usually operate at very low electric field, e.g., less than several volts per mm of the thin-, thick- or bulk-type sensor materials. The resistance or conductance of material is capable to be changed so that it is used to detect changes induced by the gases of interest. In case of varistor-type sensors, the breakdown voltage shift induced by the gases of interest is regarded as the measured of the gas sensitivity. In the present case, non-linear current–voltage characteristics of the sensor materials is measured under relatively high electric fields, and then the magnitude of breakdown voltage shift induced by the gases of interest is a direct measure of the gas sensitivity.

Here is important to emphasize that porous ZnO-based materials can also be used as varistor-type sensor. The breakdown voltage of porous ZnO-based varistors shifted to a lower electric field upon exposure to reducing gases, such as H_2,[133] in the temperature range of 300–500 °C. In contrast, the breakdown voltage of the ZnO-based varistor-type sensor shifted to a higher eletric field upon exposure to oxidizing gases, such as O_3 and NO_2.[135] Non-ohmic behavior of dense ZnO- and SnO_2-based varistor are very sensitive to thermal treatments in oxygen- and nitrogen-rich atmospheres and certain similarities arises here between dense and porous SnO_2-based ceramics or ZnO-based ceramics.[64] Concerning dense ceramic materials it was proposed that the grain-boundary region has a "p-type semiconductor nature" (due to metal transition atoms segregated at the grain boundary), while the bulk has an "n-type semiconductor nature" (SnO_2-, ZnO-based varistor matrix). This configuration enables electrons to become localized on the surfaces, giving rise to a negative surface (negative interfacial states) and as a result, electron depletion layers are formed and act as potential barriers. The potential barriers have a Schottky-like nature due to negative interfacial states, the selfsame nature often found in all metal oxide varistors and in most metal oxide gas sensors at higher temperatures.[135,128,133,134,106] It is important to note here that for varistor-type sensor the mechanism is very similar, however, the formation of the Schottky-type barrier and density states values are temperature-dependent being used as a probe for gas sensing, while in the dense traditional varistor applications, the parameters of the barrier are fixed at low temperature and is changed only during a re-sintering or thermal treatment at high temperatures in different atmospheres.[30,79,53,54,62] The influence of oxidizing gases during thermal treatments for dense SnO_2-based varistors was already illustrated in Fig. 13. Considering that Schottky-type barrier formed at grain boundary are dependent of the density of metal atoms segregated at grain boundary and also of oxygen species density at this region, according to what was discussed in Refs. 6,30,46,50,62,64,79 annealing under a reducing atmosphere (N_2, Ar or vacuum) eliminates excess oxygen, thereby, decreasing the non-linear electrical properties of the material. The process is reversible so that an annealing under an oxidizing atmosphere (O_2-rich atmosphere) at high temperature may increase again the content of oxygen at grain boundary, recovering the previous non-ohmic behavior. Fig. 13 shows the reversibility of the Schottky-type barrier for SnO_2-based varistor after thermal treatment at reducing and oxidizing atmosphere. Thermal treatment in reducing/oxidizing atmospheres at higher temperature for dense SnO_2-based polycrystalline ceramics is comparable to that found in SnO_2 varistor-type sensor. However for SnO_2-based dense varistor ceramics to alter the grain-boundary nature, which alter their non-ohmic behavior, it is necessary to impose an oxygen diffusion that occurs due to the fact that an oxygen diffusion throughout the grain boundary is likely necessary to alter the physical chemistry of the junction. In other words, this is probably a temperature activated process which might be controlled by O^{2-} ions diffusion and interfacial reaction. Therefore, once the transport mechanism is activated due to O^{2-} interface reaction and the content of oxygen species at the grain boundary can be controlled by the concentration of oxygen in the gas-phase and also by the content of metal segregated at grain boundary, according to the approach given in Ref. 64. On the other hand, in varistor-type sensor based on SnO_2, the Schottky-type barrier parameters can be altered by a physical adsorption process because in this case, the surface of the SnO_2crystal are exposed directly to the gases of interest whose molecules adsorbate on the crystal surface and boundaries (the junction is between the SnO_2surface and the gas-phase, which can be altered by altering just the equilibrium between the surface species and gaseous species). In other words, this is not a solid state chemical reaction as in the previous case, but it is a physical and reversible reaction in the conditions of the experiment or temperature operation of the varistor-sensor device.

8. Perovskite related polycrystalline non-ohmic devices

The $SrTiO_3$ is a very traditional polycrystalline device presenting non-ohmic behavior.[5,136,137] The effect of reducing atmosphere obeys similar trends found in ZnO- and SnO_2-based systems, as was already studied in the past.[5]

Other perovskite-type materials, i.e., $CaCu_3Ti_4O_{12}$(CCTO) has attracted considerable attention recently thanks to its ultrahigh dielectric property,[138,139,140,141,142] whose origin has been investigated exhaustively. Currently, the most widely accepted hypothesis is that this ultrahigh dielectric property originates from extrinsic defects caused by barrier-layer capacitances associated to internal barrier domains inside the grain.[140,143] In addition to the intriguing and remarkable dielectric property, Chung et al.[144] have observed that a large potential barrier exists intrinsically in the grain-boundary region, causing the existence of non-ohmic behavior combined with the ultrahigh dielectric property. Marques et al.[145] showed that, in CCTO systems, this non-ohmic property depends on the oxygen heat treatment, which increases low frequency capacitance values as a function of oxygen partial pressure. A similar behavior is observed in metal oxide varistor systems, leading to the inference that a Schottky-type barrier is probably the potential barrier type responsible for non-ohmic properties and that it must be located at grain-boundary junctions.[64]

Corroborating the trends for the existence of internal barrier layer,[141] ac-conductivity studies as a function of temperature of $CaCu_3Ti_4O_{12}$ polycrystalline ceramics lead to the interpretation that conductivity are associated with electrical charge carrier motion (ions or vacancies).[146] Furthermore, the long range migration of charge carriers within the ceramic is restricted by two kinds of insulating barriers, namely, grain boundaries and domain boundaries.[146] The potential barriers associated with these boundaries lead to two anomalies in conductivity response and three frequency-dependent contributions to conductivity: long range diffusion of carriers, carrier migration localized within grains, and carrier migration localized within domains.[146]

Furthermore, dielectric properties in CCTO systems are highly sensitive to processing parameters, and dielectric constant values from about $10^2$to about 10^6 have been reported.[147] Besides, non-linear coefficient values from $\sim$ 10 to $\sim$ 900 have also been reported as a consequence of different processing strategies.[144] Although a correlation between high dielectric and non-ohmic properties does appear to exist[144,145,9] it is not always observable. Therefore, it is still not evident if the non-linear electrical response is directly related to the extrinsic mechanism responsible for the ultrahigh dielectric properties, a mechanism still poorly understood,[144,142,140,145,147,148,149,150] despite the fact that it appears to be related to barrier-layer capacitances.[151] Based on this picture, it can be inferred that more than one type of barrier can contribute to the extrinsic dielectric properties: different internal barriers inside the grain and even Schottky-type barriers in the grain-boundary junctions.[151,144,152] Changes in the compositions of CCTO polycrystalline systems may help explain how chemistry and stoichiometry affect these properties. In this context, Lin et al.[9] recently investigated TiO_2-rich CCTO systems and found high dielectric properties. However, the non-linear electrical properties declined sharply compared to traditional compositions, reaching low values of around 7.[9] Moreover, an X-ray diffraction analysis indicated that the excess of TiO_2 precipitated as a second phase.[9] Additional important information provided by Li et al.'s work is that an increase in TiO_2 content decreases the dielectric constant of polycrystalline materials.

It have been shown that the initial cation stoichiometry is a significant variable that determines the overall *I*– *V* relationship of Sc-doped CCTO polycrystals, which can exhibit either strong non-linear characteristics as in the undoped CCTO or a nearly Ohmic behavior with negligible nonlinearity.[153] Such a remarkable difference in the electrical behavior has been also demonstrated to closely correlate to whether or not a large potential barrier is present at the grain boundaries. Based on the experimental measurements, plausible substitutional sites of Sc ions in the unit cell, depending on the initial composition, were suggested, although a further investigation on the lattice stability with a different stoichiometry is necessary.[153]

The dopant role on the electric and dielectric properties of the perovskite-type $CaCu_3Ti_4O_{12}$compound is evident and influence very much both properties: dielectric and non-ohmic.[142] Impedance spectroscopy measurements show that the relevant permittivity value attributed to the sintering is due to grain-boundary effects. The grain-boundary permittivity value of the pure $CaCu_3Ti_4O_{12}$ can be increased of 1–2 orders of magnitude by cation substitution on Ti site and/or segregation of CuO phase, while the bulk permittivity keeps values around 90–180.

As a consequence that the properties of $CaCu_3Ti_4O_{12}$ material is very dependent of the stoichiometry, it is very expected that effect of processing on the dielectric properties must be equivalently important. The effect of processing in $CaCu_3Ti_4O_{12}$ compound prepared by using conventional ceramic solid state reaction processing techniques was performed by Bender and Pan.[147] Powders mixed via mortar and pestle yielded $CaCu_3Ti_4O_{12}$ compound with a room temperature permittivity of 11,700 and a loss of 0.047. However, attrition-milled powders led to $CaCu_3Ti_4O_{12}$ compound with permittivities close to 100,000 which are in the same range reported for single crystal.[149,140] Increasing sintering temperature in the range from 990 to 1050 ° C led to an increase in both the dielectric constant (714–82,450) and loss (0.014–0.98).[147] Increasing sintering times also led to substantial improvements in permittivity. Grain size and density differences were not large enough to account for the enhancement in dielectric constant.[147] The colossal effective dielectric constant of close to 1 million at room temperature was measured after annealing in flowing argon at 1000 °C. Based on the observations, it is believed that the primary factor affecting dielectric behavior is the development of internal defects.[147] The authors suggested that the higher defect concentration within the 'core' of a grain results in higher conductivity of the 'core' and therefore,[147] higher effective dielectric constant but also higher loss.

Therefore, changes in the compositions of CCTO polycrystalline systems may help explain how chemistry and stoichiometry affect these properties. In this context, Lin et al.[154] recently investigated TiO_2-rich CCTO systems and found high dielectric properties.[154] However, the non-linear electrical properties declined sharply compared to traditional compositions, reaching low values of around 7.[154] Moreover, an X-ray diffraction analysis indicated that the excess of TiO_2 precipitated as a second phase.[154] Additional important information provided by

Li et al.'s[154] work is that an increase in TiO_2 content decreases the dielectric constant of polycrystalline materials.

It is possible to infer that the excess of Ti does not decrease the dielectric constant values as markedly as Ca atoms do.[154] On the other hand, an excess of Ca atoms causes an increase of non-ohmic properties compared with Ti atoms existing in excess in traditional CCTO compositions. Evidently, based on these combined results, it can be stated that the relationship between dielectric properties and non-ohmic behavior pointed out by Chung et al.[144] is not so easy to be established. One may argue that the non-linear coefficient values and dielectric constant obtained by Chung et al.[144] are much higher than the value reported by Li et al.[154] or equivalent to the value presented in work of Ramírez et al.,[155] in which an investigation was made into the non-ohmic and dielectric properties of a $Ca_2Cu_2Ti_4O_{12}$ perovskite-type system. Compared to the traditional $CaCu_3Ti_4O_{12}$-based composition, the imbalance between the Ca and Cu atoms caused the formation of a polycrystalline system presenting about 33.3 mol% of $CaCu_3Ti_4O_{12}$ (traditional composition) and about 66.7 mol% of $CaTiO_3$.[155] For non-ohmic properties, the effect of this Ca and Cu atom imbalance was that a non-linear electric behavior of about 1500 was obtained. This high non-linear electrical behavior emerged in detriment to the ultrahigh dielectric property frequently reported.[155]

With regard to the dielectric constant values, the value found by Chung et al.[144] is indisputably higher than that reported by Li et al.,[154] but this does not hold true with respect to the non-ohmic value obtained for the modified CCTO studied by Ramírez et al.[155] For instance, Chung et al.[144] found a value of 900 using a current range of 5–100 mA. Generally, non-linear coefficient values are reported for non-ohmic devices using current densities starting at 1 mA/cm^2 and ranging up to 10 mA/cm^2. It is very important, when dealing with non-ohmic properties to take care about the region where the non-linear coefficient value is calculated. For instance, it was report an value of 65 for the traditional current density range of 1–10 mA/cm^2 for the modified CCTO system.[155] On the other hand, the non-linear coefficient value for the same system can reach values even higher than 900 if one considers, for example, a current range of 3–30 mA.[155] For instance, in this current range, it was found a non-linear coefficient value of about 1500. This result reinforces the argument that it is not as easy to establish the correlation between non-ohmic and ultrahigh dielectric properties as Chung et al. suggest,[144] although the non-ohmic properties can contribute to the total dielectric constant value.[156]

Based on dielectric spectroscopy analysis three relaxation process is possible to be observed in CCTO systems and the contribution of grain boundary is evidently separated from that of bulk grain.[156] The dielectric spectroscopy analysis was performed in CCTO systems presenting low non-ohmic properties, and the grain's internal domain was evaluated separately from the contribution of barrier-layer capacitances associated with Schottky-type barriers in this type of material.[156] The effect of oxygen-rich atmosphere and high cooling rate were evaluated, revealing a strong increase in the dielectric properties of the $CaCu_3Ti_4O_{12}$ system under these conditions. This effect was attributed to a chemical change in the grain's internal domain, which may be considered as an internal barrier-layer capacitance of the polycrystalline material.[156]

With regard to the approximately fivefold increase in the dielectric properties caused by the high cooling rate or oxygen atmosphere during sintering, it can be inferred that both treatments exert a particularly marked influence on the grain's internal domain. Hence, they are able to increase the number of "active" domains, so that the cause of the strong increase in the dielectric properties is here mainly related to the number of "active" internal domains.[156] The chemistry of dielectric internal domains most likely depends on the oxygen and cooling rates to increase its effectiveness. In that particular context,[156] in which the non-ohmic properties are not very strong, the grain-boundary contribution is lower than the total dielectric response. For instance, the contribution of the grain-boundary effect represents about 10,000 out of the total value of 50,000 in the case of the sample sintered in an oxygen-rich atmosphere and cooled. In the case of the sample sintered in ambient air, the contribution is about 2000 out of a total of 9000.[156]

Very recently, the complex analysis of dielectric/capacitance was very useful applied to separate different polarization contributions existing in CCTO polycrystalline ceramics.[157] It was used this type of spectroscopic analysis to separate the bulk's dielectric dipolar relaxation contributions from the polarization contribution due to space charge in the grain boundaries of a $CaCu_3Ti_4O_{12}/CaTiO_3$ polycrystalline composite system.[157] The bulk dielectric dipolar relaxation was attributed to the self-intertwined domain structures[151] from $CaCu_3Ti_4O_{12}$ phase coupled to dipole relaxation from the $CaTiO_3$ phase, while the space charge relaxation was attributed to the Schottky-type potential barrier responsible for the highly non-ohmic properties observed in this composite polycrystalline system.[157]

9. Future and prospects concerning technological application of tin dioxide-based varistors

There are many possibilities concerning SnO_2-based polycrystalline ceramics for applications as VDR, i.e., varistor systems. Particularly it still important to work on the development of low voltage SnO_2varistors. For such purpose, solid state compounds based on the mixing of SnO_2 and TiO_2 are very attractable. As commented previously, the TiO_2 are capable to increase grain size of the compounds.[54,53] In general, the most difficulty found for obtaining SnO_2 low voltage based varistor system is related to the grain growth and new densifying dopants which lead to high densification and grain growth at the same time. Bi_2O_3 as dopant is also capable to increase grain size of the devices.[58,107,56] New systems with such feature must be tested for this purpose. Particularly, solid-state solution of SnO_2 and TiO_2 arises as a viable solution, as was discussed in Section 6 and commented previously here.

Systems such as $SnO_2{\cdot}MnO$, $SnO_2{\cdot}ZnO$- and $SnO_2{\cdot}$ CoO ·MnO-based varistors have been studied in detail. Particularly, it was found that MnO and ZnO plays the same role as CoO does,[27] however the microstructural differences are great. The non-ohmic properties of SnO_2 have also aroused the interest

of different researches concerning the influence of densification of the system on the non-ohmic features.[158,159,33] Indeed, it was studied both the chemical processing[158] and the addition of ZnO in place of CoO[159] and equivalent non-ohmic properties were obtained. It should be emphasized here that non-ohmic $SnO_2{\cdot}CoO$-based systems possess a more homogeneous microstructure than that of ZnO $\cdot Bi_2O_3$, which facilitates microstructural control during the sintering stage. Hence, it was proved to be a good material to study the mechanism of the formation of the Schottky-type potential barrier that appears in polycrystalline semiconductor systems, specially because the influence of intergranular layer is minimal on the frequency response, according to what was discussed in Section 3. The exact role of dopants in ZnO-based varistor ceramics has so far not been clarified, precisely due to its complex microstructure.[2] At this point, the SnO_2-based varistors present an enormous advantage over the ZnO varistors, owing to their simple microstructure and high nonlinearity with small concentrations of dopants. This would also contribute toward an understanding of the mechanisms of degradation of these systems and the improvement of their performance and durability. From the commercial standpoint, SnO_2 is a strong candidate to compete with ZnO varistors since the raw material is less environmental dangerous. There are several countries in which the manipulation of ZnO has being prohibited (and some dopants such as Bi_2O_3). This cause the limitation in the manufacturing of ZnO-based varistors. Another point that favors the use of SnO_2-based compositions is their shorter thermal treatment cycles, capable also to compensate the higher sintering temperature. Moreover, the SnO_2-based systems require smaller amounts of costly raw material (used as dopants), such as CoO, to achieve the same non-ohmic properties and greater resistance to degradation.[101] The two main disadvantage of SnO_2-based varistor compared with ZnO is the high temperature for sintering of the blocks and the higher cost of SnO_2 raw material comparatively to ZnO.

However, the higher cost of SnO_2 compared to ZnO can be overcome considering the fact that there are a higher number of effective potential barrier in SnO_2 compared to ZnO (as discussed in Section 5). This fact render a different nominal voltage for $SnO_2$and the blocks can be fabricated in lower dimension. Therefore, for the $SnO_2{\cdot}CoO$-based varistor system there is the possibility to decrease the dimension of final devices in at least 70%, according to some technological studies made in Brazil in cooperation with some companies of other countries. The decrease on the dimension of the devices has a lot of advantages and are capable to render at least equivalent prize in the final device to that found in ZnO. Specially in Brazil, there are a great interest in the development of new varistor systems because in that country there is the highest rate of atmospheric discharge per year in the world, mainly in the most competitive and economically important region of the country, i.e., in southeast region.

Finally, it is important to point out the remarkable difference on the thermal conductivity of SnO_2-based varistor when it is compared with the other two ZnO commercial samples[31] which could be evidenced in Fig. 16. The SnO_2-based varistor system present thermal conductivity up to two times higher than that found on ZnO-based commercial varistor (in Fig. 16, the $SnO_2{\cdot}CoO$-based varistor thermal conductivity is compared with two distinct ZnO commercial samples) according to Ref. 31.

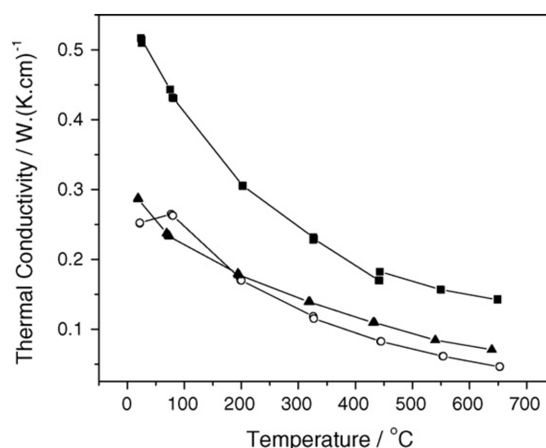

Fig. 16. Thermal conductivities of commercial ZnO samples and SnO_2sample. (■) $SnO_2{\cdot}CoO$-based varistor, (○) ZnO-based varistor, commercial sample number 1 (ZnO-C1) and (▲) ZnO-based varistor, commercial sample number 2 (ZnO-C2).

On the one hand, as foreseen, taking into account the experimental error, the values of thermal conductivity to different ZnO commercial samples can be considered equivalent[31] even when compositions changes greatly which means that the matrix plays the major role. On the other hand, the values of thermal conductivity of SnO_2 sample is almost 70% higher than the value found in ZnO commercial samples at lower temperature and almost 85% higher as temperature increase up to 923 K. Thus, SnO_2-based varistor system presents several advantages on the commercial ZnO-based varistor as already commented. Once the electrical properties are equivalent, other physical properties such as thermal conductivity favor the use of SnO_2-based varistor. The comparative results of physical and chemistry properties of commercial ZnO- and SnO_2-based varistor still remain to be deeply studied specially concerning degradation features of the non-ohmic properties. However, preliminary studies (to be still published in near future) have been shown that puncture failure associated with thermal runaway is not observed in $SnO_2{\cdot}CoO$-based system. This occurs probably because of the existence of a higher amount of active barrier so that the current can be better distributed in the device. Furthermore, the high capability of energy dissipation, due to higher thermal conductivity, avoid this kind of thermal–mechanical failure. The thermal runaway occurs as a consequence of current localization in a dielectric or semiconductor. The conceptual picture is a positive feedback mechanism in which the current localization occurs along some path through the microstructure with the higher current density leading to enhanced local Joule heating. Therefore, it is believed that the existence of a high amount of potential barrier per volume in $SnO_2{\cdot}CoO$-based VDR system allied with the higher thermal conductivity is capable to avoid the current localization, capable of enhancing the local Joule heating. Another consequence of the high homogeneity of the microstructure

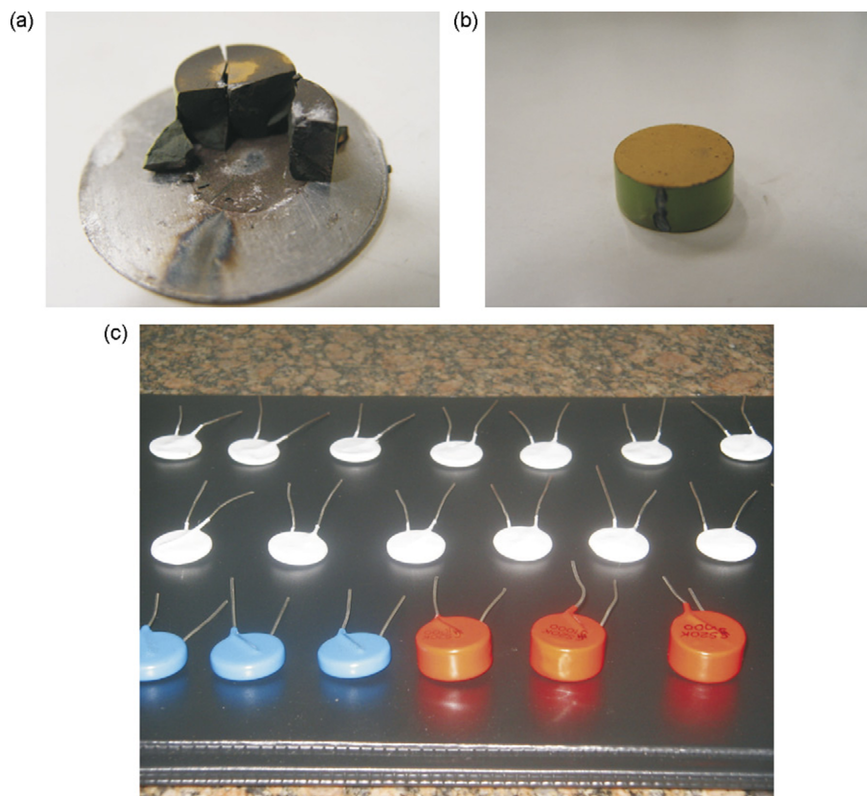

Fig. 17. (a) Failure of a commercial ZnO-based varistor system subject to pulsing loading. In this case it is possible to observe puncture failure. (b) A SnO_2 prototype varistor subjected to the same pulsing loading. Some slight changes on the *I*– *V* and non-ohmic features are affected, but no puncture failure is observed. For higher pulsing loading the failure of the isolation occurs. The project of the device must be changed. This is a much more engineering technological concerning study than ceramic material problem. (c) Illustrative photography of some SnO_2-based varistor prototype under study for future commercialization step.

and potential barrier distribution of the $SnO_2{\cdot}CoO$-varistor system lead to the fact that the statistical distribution of the energy handling is shorter from one varistor tested piece to another, comparing to that found in ZnO commercial samples.

Another important technological aspect related to SnO_2-based varistor system is concerned to the electrical and microstructural properties of the these systems sintered at 1300 ° C for 1 h, i.e., they are minimally affected by the area/volume (*A* /*V*) ratio. This prove that it is a very stable system and that the losses of dopant elements due to volatilization is minimized (a study to be also published in a near future), specially compared to ZnO traditional and commercial systems.[160,161] This is an advantage on industrial level because it allows varistor production with multiple geometries. Samples with small *A* /*V* ratio ($2.8\,cm^{-1}$) present minimum variations in microstructural and electrical properties. These variations are due to a non-uniform temperature distribution along the transversal section of the sample. The most sensitive parameter is the leakage current, which depends on thermal treatment and is related to the dopant evolution. The samples sintered at temperatures above 1300° C degrade the electrical properties, probably due to higher rate of CoO evaporation.

The Bi_2O_3 volatilization problem have conducted to new processing strategies in order to control the excessive volatilization of Bi_2O_3 in varistor during the sintering.[162] Concerning SnO_2-based varistor, the problems with Bi_2O_3 volatilization are completely overcome. Different compositional systems have been employed to improve the degradation and stability of ZnO-based varistor system[102,163,164] and the degradation mechanism and resistivity are been still tested.[114]

In Fig. 17 is it shown the degradation pulse loading in ZnO- and SnO_2-based varistor systems, comparatively (see parts (a) and (b) of Fig. 17). The ZnO is a commercial sample that suffer punctual failure, being completely destroyed. For the same pulsing loading, the SnO_2-based varistor system was affect just in its *I*– *V* characteristic, specially suffering an increasing of the leakage current. Thermal treatments are capable to recover the original properties of these devices. For more intense pulses the failure occurs in the isolation, showing that it is very important to work on the project of the device to take all the benefits of the SnO_2 material for VDR commercial application.

Therefore, it is important to comment that the electrical properties of ZnO and SnO_2 are quite equivalent albeit the microstructure and thermal properties favors applicability of SnO_2-based varistor as a future commercial device to compete with ZnO-based varistor. At this point it depends on regional interest and technological challenges to be achieved by the companies competing in this field. SnO_2-based varistor would be adequately projected for high field devices, where low dimensions of the devices may be important, allied to the high durability of the surge arrester blocks.

10. Conclusions

Polycrystalline ceramic materials have been studied for use as protectors against current (or voltage) overload in electronic circuits or as electrical discharge devices in power distribution systems. The most exhaustively studied and widely commercialized system to date has been the polycristalline ZnO-based system. Over the past few years, several researcher has been developed different metal oxide varistor system. After ZnO-based commercial compositions, the SnO_2-based compositions appears to be most studied. Several commercial and technological studies show that this system is capable to compete commercially with ZnO-based varistor system. This new system presents a coefficient of nonlinearity between current and voltage equivalent to that of ZnO, with the advantage of possessing similar properties and requiring lower concentrations of dopants and shorter thermal treatment cycles during its processing. The more homogeneous microstructure of SnO_2 has aroused much interest, particularly since it facilitates studies of the chemical nature of the potential barrier, whose physical nature is responsible for these systems' non-linear properties.

Acknowledgments

The authors are grateful to the Brazilian research funding institutions FAPESP and CNPq for their financial support of this work. We would like to thank very much Prof. Robert Freer for his help with Fig. 9. We are also very grateful to the Dr. MiguelÁngel Ramírez by providing details and information concerning Fig. 17 and other information concerning to still unpublished data. Paulo R. Bueno would like also to thank his wife for patient and very important helping with some drawing of the schematic figures observed along this text.

References

1. Levinson, L. M. and Philipp, H. R., *Ceramic Bulletin*, 1985, **64**, 639.
2. Clarke, D. R., *Journal of American Ceramic Society*, 1999, **82**, 485.
3. Greuter, F. and Blatter, G., *Semiconductor Science Technology*, 1990, **5**, 111.
4. Stucki, F. and Greuter, F., *Applied Physics Letter*, 1990, **57**, 446.
5. Nakano, Y. and Ichinose, N., *Applied Physics Letter*, 1990, **12**, 2910.
6. Bueno, P. R., Camargo, E., Longo, E., Leite, E. R., Pianaro, S. A. and Varela, J. A., *Journal of Materials Science Letters*, 1996, **15**, 2048.
7. Yan, M. F. and Rhodes, W. W., *Applied Physics Letters*, 1982, **40**, 536.
8. Pennewiss, J. and Hoffmann, B., *Materials Letters*, 1990, **9**, 219.
9. Li, J. Y., Li, S. T. and Alim, M. A., *Journal of Materials Science: Materials in Electronics*, 2006, **17**, 503.
10. Navale, S. C., Murugan, A. V. and Ravi, V., *Ceramics International*, 2007, **33**, 301.
11. Yang, X. S., Wang, Y., Dong, L., Chen, M., Zhang, F. and Qi, L. Z., *Materials Science and Engineering B: Solid State Materials For Advanced Technology*, 2004, **110**, 6.
12. Zang, G. Z., Wang, J. F., Chen, H. C., Su, W. B., Wang, C. M. and Qi, P., *Journal of Materials Science*, 2004, **39**, 4373.
13. Pianaro, S. A., Bueno, P. R., Longo, E. and Varela, J. A., *Journal of Materials Science Letters*, 1995, **14**, 692.
14. Brankovic, G., Brankovic, Z., Santos, L. P. S., Longo, E., Davolos, M. R. and Varela, J. A., *Advanced Powder Technology III of Materials Science*, 2003, **416-4**, 651–655.
15. Santhosh, P. N. and Date, S. K., *Bulletin of Materials Science*, 1996, **19**, 713.
16. Levinson, L. M. and Philipp, H. R., *J. Appl. Phys*, 1971, **46**, 1332.
17. Matsuoka, M., *Japan Applied Physics Letter*, 1971, **10**, 736.
18. Matsuoka, M., *Japan Applied Physics Letter*, 1975, **10**, 736.
19. Mahan, G. D., Levinson, L. M. and Philipp, H. R., *Applied Physics Letter*, 1979, **50**, 2799.
20. Matsuoka, M., Masuyama, T. and Lida, Y., *Japan Applied Physics Letter*, 1969, **8**, 1275.
21. Valeyev, K. S., Knayazev, V. A. and Drozdov, N. G., *Electrichestro*, 1964, **4**, 72.
22. Mukae, K., Tsuda, K. and Nagasawa, I., *Japan Applied Physics Letter*, 1977, **16**, 1361.
23. Mukae, K., Tsuda, K. and Nagasawa, I., *Applied Physics Letter*, 1979, **50**, 4475.
24. Alim, M. A., Seitz, M. A. and Hirthe, R., *Journal of Applied Physics*, 1988, **63**, 2337.
25. Levinson, L. M. and Philipp, H. R., *Journal of Applied Physics*, 1976, **47**, 1117.
26. Mukae, K., *American Ceramic Society Bulletin*, 1987, **66**, 1329.
27. Anastasiou, A., Lee, M. H. J., Leach, C. and Freer, R., *Journal of the European Ceramic Society*, 2004, **24**, 1171.
28. Pianaro, S. A., Bueno, P. R., Longo, E., and Varela, J. A. National Institute of Patents, Patent Under Number 9600174-7A, 1995.
29. Cerri, J. A. Master's Thesis Universidade Federal de São Carlos, 1995.
30. Bueno, P. R., de Cassia-Santos, M. R., Leite, E. R., Longo, E., Bisquert, J., Garcia-Belmonte, G. and Fabregat-Santiago, F., *Journal of Applied Physics*, 2000, **88**, 6545.
31. Bueno, P. R., Varela, J. A., Barrado, C. M., Longo, E. and Leite, E. R., *Journal of the American Ceramic Society*, 2005, **88**, 2629.
32. Cerri, J. A., Leite, E. R., Gouvêa, D., Longo, E. and Varela, J. A., *Journal of Material Science Letter*, 1996, **79**, 799.
33. Castro, M. S. and Aldao, C. M., *Journal of European Ceramic Society*, 1998, **18**, 2233.
34. Jarzebski, Z. M. and Marton, J. P., *Journal of Electrochemical Society*, 1976, **123**, 199.
35. Fagan, J. G. and Amarakoon, V. R. W., *American Ceramic Society Bulletin*, 1993, **72**, 119.
36. Chopra, K. L., Major, S. and Pandya, P. K., *Thin Solid Films*, 1983, **102**, 1.
37. Duhn, J. G., Jou, J. W. and Chiou, B. S., *Journal of Electrochemical Society*, 1989, **136**, 2740.
38. Semancik, S. and Fryberger, T. B., *Sensors & Actuators B*, 1990, **1**, 97.
39. Göpel, W. and Shierbaum, K. D., *Sensors & Actuators B*, 1995, **26-27**, 1.
40. Seiyama, T., Yamazae, N. and Arai, H., *Sensors & Actuators B*, 1983, **4**, 85.
41. Ihokura, K., Tanaka, K. and Murakami, N., *Sensors & Actuators B*, 1983, **4**, 607.
42. Traversa, E., *Journal of American Ceramic Society*, 1995, **78**, 2625.
43. Park, S. J., Hirota, K. and Yamamura, H., *Ceram International*, 1984, **10**, 116.
44. Islam, M. H. and Hogarth, C. A., *Journal of Material Science Letter*, 1989, **8**, 986.
45. Gouvêa, D. PhD Thesis, Universidade Federal de São Carlos, 1996.
46. Leite, E. R., Nascimento, A. M., Bueno, P. R., Longo, E. and Varela, J. A., *Journal of Materials Science: Materials in Electronics*, 1999, **10**, 321.
47. Santos, P. A., Maruchin, S., Menegoto, G. F., Zar, A. J. and Pianaro, S. A., *Materials Letters*, 2006, **60**, 554.
48. Dibb, A., Tebcherani, S. M., Lacerda, W., Santos, M. R. C., Cilense, M., Varela, J. A. and Longo, E., *Materials Letters*, 2000, **46**, 39.
49. Menegotto, G. F., Pianaro, S. A., Zara, A. J., Antunes, S. R. M. and Antunes, A. C., *Journal of Materials Science: Materials in Electronics*, 2002, **13**, 253.
50. Oliveira, M. M., Bueno, P. R., Cassia-Santos, M. R., Longo, E. and Varela, J. A., *Journal of the European Ceramic Society*, 2001, **21**, 1179.
51. Wang, Y. J., Wang, J. F., Li, C. P., Chen, H. C., Su, W. B., Zhong, W. L., Zhang, P. L. and Zhao, L. Y., *European Physical Journal: Applied Physics*, 2000, **11**, 155.

52. Li, C. P., Wang, J. F., Su, W. B., Chen, H. C., Wang, W. X., Zang, G. Z. and Xu, L., *Ceramics International*, 2002, **28**, 521.
53. Bueno, P. R., Cassia-Santos, M. R., Simoes, L. G. P., Gomes, J. W., Longo, E. and Varela, J. A., *Journal of the American Ceramic Society*, 2002, **85**, 282.
54. Bueno, P. R., Leite, E. R., Bulhões, L. O. S., Longo, E. and Paiva-Santos, C. O., *Journal of the European Ceramic Society*, 2003, **26**, 887.
55. Bernik, S. and Daneu, N., *Journal of the European Ceramic Society*, 2001, **21**, 1879.
56. Daneu, N., Recnik, A., Bernik, S. and Kolar, D., *Journal of the American Ceramic Society*, 2000, **83**, 3165.
57. Wang, Y. G., Wang, J. F., Chen, H. C., Zhong, W. L., Zhang, P. L., Dong, H. M. and Zhao, L. N., *Journal of Physics D: Applied Physics*, 2000, **33**, 96.
58. Pianaro, S. A., Bueno, P. R., Olivi, P., Longo, E. and Varela, J. A., *Journal of Materials Science Letters*, 1997, **16**, 634.
59. Pianaro, S. A., Bueno, P. R., Olivi, P., Longo, E. and Varela, J. A., *Journal of Materials Science: Materials in Electronics*, 1998, **9**, 159.
60. Antunes, A. C., Antunes, S. R. M., Pianaro, S. A., Rocha, M. R., Longo, E. and Varela, J. A., *Journal of Materials Science: Materials in Electronics*, 1998, **17**, 577.
61. Bueno, P. R., Pianaro, S. A., Pereira, E. C., Bulhoes, L. O. S., Longo, E. and Varela, J. A., *Journal of Applied Physics*, 1998, **84**, 3700.
62. Cassia-Santos, M. R., Bueno, P. R., Longo, E. and Varela, J. A., *Journal of the Eurpean Ceramic Society*, 2001, **21**, 161.
63. Glot, A. B. and Zloblin, A. P., *Inorganic Materials*, 1989, **25**, 322.
64. Bueno, P. R., Leite, E. R., Oliveira, M. M., Orlandi, M. O. and Longo, E., *Applied Physics Letters*, 2001, **79**, 48.
65. Sonder, E., Austin, M. M. and Kinser, D. L., *Journal of Applied Physics*, 1983, **54**, 3566.
66. Glot, A., Di Bartolomeo, E., Gaponov, A., Polini, R. and Traversa, E., *Journal of the European Ceramic Society*, 2004, **24**, 1213.
67. Glot, A. B., *Journal of Materials Science: Materials in Electronics*, 2006, **17**, 755.
68. Glot, A. B., *Journal of Materials Science*, 2006, **41**, 5709.
69. Glot, A. B. and Skuratovsky, I. A., *Materials Chemistry and Physics*, 2006, **99**, 487.
70. Shim, Y. and Cordaro, J. F., *Journal of American Ceramic Society*, 1988, **71**, 184.
71. Shim, Y. and Cordaro, J. F., *Journal of Applied Physics*, 1988, **64**, 3994.
72. Bueno, P. R., Varela, J. A., and Longo, E. 2007.
73. Jonscher, A. K. and Robinson, M. N., *Solid-State Electronics*, 1988, **31**, 1277.
74. Jonscher, A. K., *Solid-State Electronics*, 1993, **36**, 1121.
75. León, C., Martin, J. M., Santamaría, J., Skarp, J., González-Díaz, G. and Sánchez-Quesada, F., *Solid-State Electronics*, 1996, **79**, 7830.
76. Alim, M. A., *Journal of Applied Physics*, 1989, **74**, 5850.
77. Ezhilvalavan, S. and Kutty, T. R. N., *Applied Physics Letters*, 1996, **69**, 3540.
78. Alim, M. A., *Journal of American Ceramic Society*, 1989, **72**, 28.
79. Bueno, P. R., Oliveira, M. M., Bacelar-Junior, W. K., Leite, E. R., Longo, E., Garcia-Belmonte, G. and Bisquert, J., *Journal of Applied Physics*, 2002, **91**, 6007.
80. Garcia-Belmonte, G., Bisquert, J. and Fabregat-Santiago, F., *Solid-State Electronics*, 1999, **43**, 2123.
81. Chiou, B. S. and Chung, M.-C., *Journal of Electronic Materials*, 1991, **20**, 885.
82. Li, H., Xu, Y., Wang, S. and Wang, L., *Applied Physics Letters*, 1994, **69**, 3540.
83. Fan, J. and Freer, R., *Applied Physics Letters*, 2007, **90**, 935111.
84. Orlandi, M. O., Bueno, P. R., Bomio, M. R. D., Longo, E. and Leite, E. R., *Journal of Applied Physics*, 2004, **96**, 3811.
85. Cox, D. F., Fryberger, T. B. and Semancik, S., Phys. *Review B*, 1998, **38**, 2072.
86. Rantala, T., Lantto, V. and Rantala, T., *Sensor & Actuators B*, 1998, **47**, 59.
87. Sato, Y., Buban, J. P., Mizoguchi, T., Shibata, N., Yodogawa, M., Yamamoto, T. and Ikuhara, Y., *Physical Review Letters*, 2006, **97**, 10.
88. Wang, C. M., Wang, J. F., Su, W. B., Chen, H. C., Wang, C. L., Zhang, J. L., Zang, G. Z., Qi, P., Gai, Z. G. and Ming, B. Q., *Materials Science and Engineering B: Solid State Materials for Advanced Technology*, 2006, **127**, 112.
89. Parra, R., Varela, J. A., Aldao, C. M. and Castro, M. S., *Ceramics International*, 2005, **31**, 737.
90. Parra, R., Maniette, Y., Varela, J. A. and Castro, M. S., *Materials Chemistry and Physics*, 2005, **94**, 347.
91. Wang, C. M., Wang, J. F. and Su, W. B., *Journal of the American Ceramic Society*, 2006, **89**, 2502.
92. Sonder, E., Austin, M. M. and Kinser, D. L., *Journal of Applied Physics*, 1983, **54**, 3566.
93. Vasconcelos, J. S., Vasconcelos, N. S. L. S., Orlandi, M. O., Bueno, P. R., Varela, J. A., Longo, E., Barrado, C. M. and Leite, E. R., *Applied Physics Letters*, 2006, **89**, 152102.
94. Antunes, A. C., Antunes, S. R. M., Pianaro, S. A., Longo, E., Leite, E. R. and Varela, J. A., *Journal of Materials Science: Materials in Electronics*, 2001, **12**, 69.
95. Antunes, A. C., Antunes, S. R. M., Zara, A. J., Pianaro, S. A., Longo, E. and Varela, J. A., *Journal of Materials Science*, 2002, **37**, 2407.
96. Dhage, S. R., Choube, V. and Ravi, V., *Materials Science and Engineering B: Solid State Materials for Advanced Technology*, 2004, **110**, 168.
97. Dibb, A., Tebcherani, S. M., Santos, M., Cilense, M., Varela, J. A. and Longo, E., *Advanced Powder Technology II, of Key Engineering Materials*, 2001, **189–1**, 161–165.
98. Dibb, A., Tebcherani, S. M., Lacerda, W., Cilense, M., Varela, J. A. and Longo, E., *Journal of Materials Science: Materials in Electronics*, 2002, **13**, 567.
99. Pianaro, S. A., Bueno, P. R., Longo, E. and Varela, J. A., *Ceramics International*, 1999, **25**, 1.
100. Varela, J. A., Cerri, J. A., Leite, E. R., Longo, E., Shamsuzzoha, M. and Bradt, R. C., *Ceram International*, 1999, **25**, 253.
101. Gouvêa, D. PhD Thesis Universidade Federal de São Carlos, 1998.
102. Nahm, C. W., *Materials Letters*, 2006, **60**, 3394.
103. Leach, C. and Vernon-Parry, K., *Journal of Materials Science*, 2006, **41**, 3815.
104. Wang, Y. J., Wang, J. F., Li, C. P., Chen, H. C., Su, W. B., Zhong, W. L., Zhang, P. L. and Zhao, L. Y., *European Physical Journal: Applied Physics*, 2000, **11**, 155.
105. Leite, E. R., Varela, J. A. and Longo, E., *Journal of Applied Physics*, 1992, **72**, 147.
106. Egashira, M., Shimizu, Y., Takao, Y. and Sako, S., *Sensors and Actuators B: Chemical*, 1996, **35**, 62.
107. Bernik, S., Zupancic, P. and Kolar, D., *Journal of the European Ceramic Society*, 1999, **19**, 709.
108. Fayat, J. and Castro, M. S., *Journal of the European Ceramic Society*, 2003, **23**, 1585.
109. Bueno, P. R., Orlandi, M. O., Simões, L. G. P., Leite, E., Longo, E. and Cerri, J. A., *Journal of Applied Physics*, 2004, **96**, 2693.
110. Parra, R., Castro, M. S. and Varela, J. A., *Journal of the European Ceramic Society*, 2005, **25**, 401.
111. Parra, R., Aldao, C. M., Varela, J. A. and Castro, M. S., *Journal of Electroceramics*, 2005, **14**, 149.
112. Li, C. P., Wang, J. F., Su, W. B., Chen, H. C., Wang, W. X. and Zhuang, D. X., *Physica B: Condensed Matter*, 2001, **307**, 1.
113. Wang, Y. J., Wang, J. F., Li, C. P., Chen, H. C., Su, W. B., Zhong, W. L., Zhang, P. L. and Zhao, L. Y., *Journal of Materials Science Letters*, 2001, **20**, 19.
114. Lee, H. J., Kim, C. D., Kang, S. H., Kim, I. W., Lee, J. S. and Chung, G. S., *Journal of the Korean Physical Society*, 2006, **49**, 2423.
115. Hirose, S., Nishita, K. and Niimi, H., *Journal of Applied Physics*, 2006, **100**, 8.
116. Simoes, L. G. P., Bueno, P. R., Orlandi, M. O., Leite, E. R. and Longo, E., *Journal of Electroceramics*, 2003, **10**, 63.
117. Sato, Y., Yamamoto, T. and Ikuhara, Y., *Journal of the American Ceramic Society*, 2007, **90**, 337.
118. Clarke, D. R., *Journal of Applied Physics*, 1979, **49**, 2407.

119. Tao, M., Bui, A., Dorlanne, O. and Loubiere, A., *Journal of Applied Physics*, 1986, **61**, 1562.
120. Vasconcelos, J. S., Vasconcelos, N. S. L. S., Orlandi, M. O., Bueno, P. R., Varela, J. A., Longo, E., Barrado, C. M. and Leite, E. R., *Applied Physics Letters*, 2006, **89**, 152102.
121. Li, C. P., Wang, J. F., Wang, Y. J., Su, W. B., Chen, H. C. and Zhuang, D. X., *Chinese Physics Letters*, 2001, **18**, 674.
122. Li, C. P., Wang, J. F., Su, W. B., Chen, H. C. and Wang, W. X., *Journal of Materials Science and Technology*, 2002, **18**, 283.
123. Li, H. Y., Luo, S. H., Tang, Z. L., Yao, W. H., Zhang, Z. T., Zhuang, Y. and Xiong, X. H., *Rare Metal Materials and Engineering*, 2002, **31**, 229.
124. Li, J. Y., Luo, S. H., Yao, W. H., Tang, Z. L., Zhang, Z. T. and Alim, M. A., *Journal of the European Ceramic Society*, 2004, **24**, 2605.
125. Li, J. Y., Luo, S. H., Yao, W. H. and Zhang, Z. T., *Materials Letters*, 2003, **57**, 3748.
126. Luo, J. J., Fang, X. Y. and Wu, M. T., *Journal of Inorganic Materials*, 2000, **15**, 93.
127. Luo, S. H., Tang, Z. L., Li, H. Y., Yan, J. P., Zhang, Z. T. and Xiong, X. Z., *Rare Metal Materials and Engineering*, 2004, **33**, 748.
128. Egashira, M., Shimizu, Y., Takao, Y. and Fukuyama, Y., *Sensors and Actuators B: Chemical*, 1996, **33**, 89.
129. Radecka, M., Pasierb, M., Zakrzewska, K. and Rekas, M., *Solid State Ionics*, 1999, **119**, 43.
130. Zakrzewska, M. R. K. and Rekas, M., *Sensor and Actuators B*, 1998, **47**, 194.
131. Jarzebski, Z. M. and Marton, J. P., *Journal of Electrochemical Society*, 1976, **123**, 299.
132. Chiang, Y.-M., Birnie, D. and Kingery III, W. D., Physical ceramics. Principles for ceramics science and engineering. *MIT Series in Materials Science and Engineering Series Statement*. John Wiley and Sons, Inc, New York, 1997.
133. Shimizu, Y., Kanazawa, E., Takao, Y. and Egashira, M., *Sensors and Actuators B-Chemical*, 1998, **52**, 38.
134. Egashira, M., Shimizu, Y., Takao, Y. and Fukuyama, Y., *Sensors and Actuators B: Chemical*, 1996, **33**, 89.
135. Egashira, M., Shimizu, Y., Takao, Y. and Sako, S., *Sensors and Actuators B: Chemical*, 1996, **35**, 62.
136. Li, J. Y., Li, B., Zhai, D. Y., Li, S. T. and Alim, M. A., *Journal of Physics D: Applied Physics*, 2006, **39**, 4969.
137. Yordanov, S. P., *International Journal of Electronics*, 1992, **73**, 301.
138. Adams, T. B., Sinclair, D. C. and West, A. R., *Advanced Materials*, 2002, **14**, 1321.
139. Adams, T. B., Sinclair, D. C. and West, A. R., *Physical Review B*, 2006, **73**, 094124.
140. Li, G. L., Yin, Z. and Zhang, M. S., *Physics Letters A*, 2005, **344**, 238.
141. Sinclair, D. C., Adams, T. B., Morrison, F. D. and West, A. R., *Applied Physics Letters*, 2002, **80**, 2153.
142. Capsoni, D., Bini, M., Massarotti, V., Chiodelli, G., Mozzatic, M. C. and Azzoni, C. B., *Journal of Solid State Chemistry*, 2004, **177**, 4494.
143. Ramirez, A. P., Subramanian, M. A., Gardel, M., Blumberg, G., Li, D., Vogt, T. and Shapiro, S. M., *Solid State Communications*, 2000, **115**, 217.
144. Chung, S. Y., Kim, I. and Kang, S., *Nature Materials*, 2004, **3**, 774.
145. Marques, V. P. B., Bueno, P. R., Simoes, A. Z., Cilense, M., Varela, J. A., Longo, E. and Leite, E. R., *Solid State Communications*, 2006, **138**, 1.
146. Li, W. and Schwartz, R. W., *Applied Physics Letters*, 2002, **89**, 242906.
147. Bender, B. A. and Pan, M. J., *Materials Science and Engineering B: Solid State Materials for Advanced Technology*, 2005, **117**, 339.
148. Kretly, L. C., Almeida, A. F. L., de Oliveira, R. S., Sasaki, J. M. and Sombra, A. S. B., *Microwave and Optical Technology Letters*, 2003, **39**, 145.
149. Subramanian, M. A., Li, D., Duan, N., Reisner, B. A. and Sleight, A. W., *Journal of Solid State Chemistry*, 2000, **151**, 323.
150. West, A. R., Adams, T. B., Morrison, F. D. and Sinclair, D. C., *Journal of the European Ceramic Society*, 2004, **24**, 1439.
151. Fang, L., Shen, M. and Yao, D., *Applied Physics A: Materials Science and Processing*, 2005, **80**, 1763.
152. Fang, T. T. and Shiau, H. K., *Journal of the American Ceramic Society*, 2004, **87**, 2072.
153. Chung, S. Y., Lee, S.-I. and Choi, J.-H., *Applied Physics Letters*, 2006, **89**, 191907.
154. Lin, Y.-H., Cai, J., Li, M., Nan, C.-W. and He, J., *Applied Physics Letters*, 2006, **88**, 172902.
155. Ramírez, M. A., Bueno, P. R., Varela, J. A. and Longo, E., *Applied Physics Letters*, 2006, 89.
156. Bueno, P. R., Ramrez, M. A., Varela, J. A. and Longo, E., *Applied Physics Letters*, 2006, **89**, 191117.
157. Bueno, P. R., Ribeiro, W. C., Ramrez, M. A., Varela, J. A. and Longo, E., *Applied Physics Letters*, 2007, **90**, 142912.
158. Santhosh, P. N., Potdar, H. S. and Date, S. K., *Journal of Materials Research*, 1997, **12**, 326.
159. Yongjun, W., Jinfeng, W., Hongcun, C., Weilie, Z., Peilin, Z., Huomin, D. and Lianyi, Z., *Journal of Physics D: Applied Physics*, 2000, **33**, 96.
160. de la Rubia, M. A., Peiteado, M., Fernández, J. F. and Caballero, A. C., *Journal of European Ceramic Society*, 2004, **24**, 1209.
161. Peiteado, M., de la Rubia, M. A., Velasco, M. J., Valle, F. J. and Caballero, A. C., *Journal of European Ceramic Society*, 2005, **25**, 1675.
162. De la Rubia Lopez, M. A., Peiteado, M., Fernandez, J. F., Caballero, A. C., Holc, J., Drnovsek, S., Kuscer, D., Macek, S. and Kosec, M., *Journal of the European Ceramic Society*, 2006, **26**, 2985.
163. Nahm, C. W., *Materials Letters*, 2006, **60**, 3311.
164. Nahm, C. W., *Materials Science and Engineering B: Solid State Materials for Advanced Technology*, 2006, **133**, 91.